Earth Science Informatics (2025) 18:211
https://doi.org/10.1007/s12145-025-01726-y

RESEARCH

Granite porosity prediction under varied thermal conditions using machine learning models

Rishabh Dwivedi[1] · Balbir Prasad[2] · PK Gautam[3] · Peeyush Garg[2,4] · Siddhartha Agarwal[2] · KH Singh[1] · TN Singh[1]

Received: 28 August 2024 / Accepted: 18 January 2025 / Published online: 29 January 2025

Abstract

Porosity estimation at high granite temperatures is essential for numerous purposes, including natural and enhanced geothermal energy production. However, these methods of determining porosity have some disadvantages, such as being labor-intensive, requiring expensive instrumentation, and taking a significant amount of time, particularly during elevated temperature treatments. This study is vital for advancing geothermal energy applications by addressing the limitations of traditional porosity estimation methods. The study introduces innovative predictive machine learning (ML) models and offers insights into practical applications for improving geothermal reservoir management and sustainability. the datasets divided into six subsets, each with a specific grain size (fine, medium, or coarse) and cooling method furnace cooling (FC) and water cooling (WC). The cooling rate has a significant impact on rock thermal stress. In this study, six ML models—Random Forest (RF), K-Nearest Neighbors (KNN), Extreme Gradient Boosting (XGBoost), Support Vector Machine (SVM), Categorical Boosting (CatBoost), and Light Gradient Boosting Machine (LightGBM)—were employed to predict models for estimating porosity at high temperatures. The multiple evaluation metrics were used to assess the suitability of these algorithms. R-squared values were calculated to assess the models' goodness-of-fit. In parallel, several error metrics such as root mean squared error (RMSE), mean absolute error (MAE), mean absolute percentage error (MAPE), root mean square relative error (RMSRE), mean absolute relative error (MARE), and percent bias (PBIAS) were evaluated to quantify the accuracy of the predictions. The performance of the ML methods exhibited considerable variability among the different datasets. Among the evaluated models, CatBoost and KNN consistently achieved higher R-squared values and lower error metrics, demonstrating their effectiveness in accurately discerning underlying patterns and reliably predicting porosity. Conversely, RF, XGBoost, and SVM yielded reasonably accurate predictions, albeit with slightly increased variability in their performance metrics across different grain size and cooling condition subsets. LightGBM demonstrates comparatively diminished prediction accuracy, since it fails to capture the complex fluctuations in rock properties over thermal heating and cooling cycles. These findings highlight the superior predictive efficacy of CatBoost and KNN, confirming their reliability as robust tools for modeling porosity in complex datasets with varied geological and environmental factors.

Keywords Machine learning (ML) · Porosity · Temperature · Heating and cooling treatment · Cooling rate

Communicated by: H. Babaie

✉ PK Gautam
pgautam.embedded@gmail.com

[1] Department of Earth Sciences, Indian Institute of Technology Bombay, Mumbai, India

[2] Department of Mining Department, Indian Institute of Technology (Indian School of Mines) Dhanbad, Dhanbad, India

[3] Mewbourne School of Petroleum & Geological Engineering, The University of Oklahoma, Norman, USA

[4] Deptartment of Electrical Engineering, Manipal University Jaipur, Jaipur, India

Abbreviations

FC	Furnace Cooling
WC	Water Cooling
RF	Random Forest
KNN	K-Nearest Neighbor
XGBoost	Extreme Gradient Boosting
SVM	Support Vector Machine
CatBoost	Categorical Boosting
LightGBM	Light Gradient Boosting Machine
RMSE	Root Mean Squared Error
MAE	Mean Absolute Error
MAPE	Mean Absolute Percentage Error
RMSRE	Root Mean Square Relative Error

MARE	Mean Absolute Relative Error
PBIAS	Percent Bias
ML	Machine Learning
EGS	Enhanced Geothermal System
LN2	Liquid Nitrogen
PSO-SVM	Particle Swarm Optimization Support Vector Machine
AdaBoost	Adaptive Boosting
CART	Classification and Regression Trees
RBFNN	Radial Basis Neural Network
MLR	Multiple Linear Regression
SVR	Support Vector Regression
FG	Fine-Grained
MG	Medium-Grained
CG	Coarse-Grained
EDA	Exploratory Data Analysis
IQR	Interquartile range
SHAP	SHapley Additive exPlanations
PDP	Partial Dependence Plot
ICE	Individual Conditional Expectation

Introduction

A naturally occurring geothermal system (known as hydrothermal) has three key characteristics: heat, fluid, and permeability at depth. The subsurface resource is heat, the delivery medium is fluid, and the fluid flow pathway is permeability. Generally, most geothermal systems are adjacent to volcanic areas where the intrusion of hot molten magma is near the surface. Typically, the preferred reservoir for geothermal energy exploitation sits at a depth of 5–6 km, boasting a temperature range of 150–900 °C (Gallup 2009; Breede et al. 2013; Shao et al. 2014). However, to increase the utilization and exploitation of geothermal resources, we developed the designed geothermal system, also known as the enhanced geothermal system (EGS). An enhanced geothermal system is a reservoir developed artificially and placed in an area containing heated rock but with inadequate or very little natural porosity, permeability, or a natural fluid flow system. Cryogenic fluids can strengthen an EGS by continuously generating new fractures, expanding pre-existing ones, and improving the reservoir's permeability. Due to their high heat capacity and poor permeability, granites are the most commonly used rock in EGS. According to Zhao (2016), the phenomenon of thermal treatment has the potential to induce the formation of microcracks in rocks through two distinct mechanisms, namely thermal cycling induced cracking and thermal gradient-induced cracking. Thermal cycling-induced cracks arise due to a disparity in the thermal expansion coefficients of adjacent mineral grains within a uniform-temperature environment. In contrast, cracks induced by thermal gradients occur when temperature differentials exceed the local grain strength, leading to thermal stresses. These properties enable the retention of heat within the granite, preventing rapid dissipation and allowing for sustained thermal energy extraction. Consequently, granite is often referred to as "hot, dry rock" in geothermal context, highlighting its ability to maintain high temperature while possessing minimal natural fluid flow pathways. The injection of cold water into heated rock can establish thermal cracks, thereby increasing the permeability and porosity of the reservoir rock (Siratovich et al. 2015; Browning et al. 2016; Kumari et al. 2018). Pumping cold water into a heated rock rapidly lowers its temperature, but the rate of cooling varies based on the rock's distance from the borehole (Isaka et al. 2018). The phenomenon of thermal stress causing the expansion and contraction of grains in response to rate of heating-cooling gradient at elevated temperatures is widely acknowledged (Chen et al. 2011; Freire-Lista et al. 2016; Su et al. 2017). In addition, critical quenching can trigger a thermal shock in rock because the physical properties are proportional to the cooling rate (Fellner and Supancic 2002). Therefore, we must investigate the accurate prediction of successful geothermal energy extraction, cooling-related porosity, and permeability characteristics of heated rock. However, in preceding decades, a detailed analysis based on laboratories and numerical investigations into reservoir rocks at different temperatures have revealed that physical and mechanical properties like porosity, permeability, elastic wave propagation, static and dynamic elastic modulus, uniaxial compressive strength, and tensile strength often drop off as the temperature rises (Heuze 1983; Chen et al. 2012, 2017, 2018; Liu and Xu 2015; Gautam et al. 2016a; b; Zhao 2016; Jha et al. 2017; Liu et al. 2019; Kang et al. 2021). The thermal damage evolution of Indian granitic rock thermally treated at various heating cooling condition have been studied (Gautam et al. 2018a, b, 2019a, b, 2021). To date, only a limited number of experimental studies have focused on investigating the influence of cooling rates on the physical and mechanical properties of granite rock, as well as their thermal damage mechanism. Kim et al. (2014) used a fan to investigate how changing temperatures (100, 200, and 300 °C) impacted the mechanical properties of sandstone. It was found that rapid cooling may decrease p-wave velocity and tensile strength while concurrently increasing porosity (Shi et al. 2020; Weng et al. 2020); Brotóns et al. (2013) performed several experiments to learn more about calcarenite's mechanical properties when heated to temperatures between 105 and 600 °C and cooled using air and water. Both the elastic modulus and uniaxial compressive strength decreased as the temperature increased Kumari et al. (2017) investigated the mechanical characteristics of Australian Strathbogie granite under the effects of high temperatures and two distinct cooling methods (rapid and slow cooling). The results of their experiments suggested that

when rock was heated to high temperatures, its strength and elastic properties declined. Furthermore, rapid cooling was found to have a more significant effect than slow cooling, resulting in greater reduction in these mechanical properties. Browning et al. (2016), examined the formation of cracks in volcanic rocks during the processes of heating and cooling. Their findings indicate that cooling rock samples exhibited significantly more cracking than those subjected to heating conditions. Zhao et al. (2018) measured Brazilian indirect tensile strength on granite specimens undergoing a cyclic thermal (heating-cooling) treatment. The study revealed a strong correlation among the tensile strength of granitic samples, grain size, heterogeneity, and temperature gradient. Liu et al. (2019), investigated the cooling effects on the mechanical behavior of fine-grained, medium-grained, and coarse-grained Australian Strathbogie granite subjected to rapid cooling in water and slow cooling in the air after having been heated to high temperatures (200, 400, 600, and 800 °C) from room temperature. Their finding indicated that rapid cooling resulted in more pronounced deformation of granite specimens, principally due to the generation of an increased number of fractures, with intragranular fractures being prevalent. Coarse-grained granite exhibited significantly more intergranular fractures compared to fine-grained and medium-grained granite fractures, but very few intragranular fractures. Additionally, when cooled to the same temperature as the other granite, granite with an uneven grain size distribution exhibited more intragranular fractures. This reduced the strength of the granite with an uneven grain size distribution. Differential expansion and contraction of minerals, particularly quartz due to its relatively high thermal expansion coefficient influence the crystal structure and heterogeneity of granites over thermal cycle. In addition to air and water cooling, the impact of liquid nitrogen (LN2) cooling has also been studied (Wu et al. 2019a, b). According to their study, LN2-cooling differs significantly from air and water cooling because it involves boiling heat transfer and causes significant temperature variations. The utilization of LN2-cooling has the potential to cause more substantial damage to the heated rocks compared to alternative cooling methods.

Thus, determining the porosity under varying cooling rates at elevated temperatures within standardized experimental conditions can be expensive and time-intensive. Moreover, the implementation requires the utilization of multiple standard samples to mitigate the potential discrepancies. Advanced techniques are required for the accurate prediction of physical properties, such as porosity at elevated temperatures and at varied cooling rates.

Machine learning (ML) has recently gained recognition as an innovative and effective tool in engineering geology (Chauhan et al. 2016; Weidner et al. 2019; Miah et al. 2020; Wang et al. 2020; Xie et al. 2021; Song et al. 2022; Eltarabily and Elshaarawy 2023; Elshaarawy and Hamed 2024; Eltarabily et al. 2024a, b; Isleem et al. 2024). The ML facilitates the study and characterization of complex multidimensional datasets that are beyond the capabilities of humans. Elshaarawy and Eltarabily (2024), predicted ground water quality by optimizing ML methods and GIS. In addition, ML techniques may also be used to obtain crucial data from laboratory investigations and computer simulations of topics in rock damage. Elshaarawy et al. (2024) utilized both ensemble and non-ensemble ML models to predict the concrete compressive strength. Researchers can utilize machine learning algorithms to examine various factors influencing porosity, such as thermal stress, differential thermal expansion, and heat-induced thermal cracks, to create precise prediction models. These models can then aid in optimizing cooling processes, enhancing the efficiency and effectiveness of granite treatment procedures. Error metrics and sensitivity analysis are essential for assessing and improving ML models. Error metrics, including root mean squared error (RMSE) and mean absolute error (MAE), and percent bias (PBIAS) measure the divergence between predicted and actual values, enabling the evaluation of model performance (Eltarabily et al. 2023). Sensitivity analysis elucidates the impact of input variables on model outputs, enhancing robustness and interpretability while finding essential characteristics and mitigating overfitting concerns (Tian et al. 2024). Collectively, these instruments offer a thorough framework for enhancing and verifying machine learning models within complex systems. Mahmoodzadeh et al. (2022) and Wang et al. (2021) have revealed that the Mode I fracture toughness of rocks was predicted using ML methods. Yan et al. (2021) proposed a hybrid model by investigating four ML approaches for predicting the crack initiation pressure in supercritical carbon dioxide fracturing. Wei et al. (2022) used three ML approaches to predict the dynamic strength of rocks under various strain rates. Hu et al. (2023) used five machine learning methods to predict the triaxial compressive strength of materials after different high-temperature treatments. These were the backpropagation neural network (BPNN), the AdaBoost-CART classification and regression tree, the support vector machine (SVM), the K-nearest neighbor (KNN), and the radial basis neural network (RBFNN). However, ML methods hardly ever address temperature-related problems. Integrating ML methods to predict the porosity of granite at elevated temperatures could provide valuable insights.

In this study, ML techniques were employed to develop predictive models for the estimation of porosity. A comprehensive evaluation of multiple algorithms was conducted, yielding critical insights into their predictive performance and potential avenues for further research. This particular research work aims to address a critical gap in the existing literature by leveraging ML to predict the porosity of granite

at elevated temperatures during different cooling treatments, ultimately contributing to the efficient and sustainable utilization of geothermal resources. The prediction of the porosity of granite rock specimens using various ML methods under varying heating-cooling conditions are crucial for the progress of sustainable geothermal energy applications. Porosity directly influences the storage, flow, and extraction efficiency of geothermal fluids, which are crucial for improving energy production and reducing operational risks. Moreover, understanding the impact of cooling treatments on the porosity of granite could improve the building of more resilient geothermal reservoirs and better their long-term performance under extreme thermal stress. This research links laboratory findings to practical applications, enhancing the reliability of predictive ML models and assisting in addressing global challenges related to energy security. The datasets used in this study were divided into six subsets based on grain size heterogeneity (fine, medium, and coarse) and different cooling conditions furnace cooling (FC) and water cooling (WC). The input features of the developed prediction model are temperature, mass loss, P-wave velocity, and S-wave velocity, and the output variable is porosity. A comprehensive dataset comprising 232 data points was obtained from laboratory experiments conducted on granite rock samples, where half of the data points were under FC conditions, and half were under WC conditions. The learning models used 75% of data points for training and the remaining 25% for evaluating the model. The rock samples were investigated in the laboratory and categorized as fine, coarse, and medium-grained based on the granular size. The predictive performance of RF, KNN, XGBoost, SVR, CatBoost, and LightGBM algorithms was systematically evaluated for porosity estimation. The predictive efficacy of the model was rigorously evaluated using the R-squared values (R^2) and multiple evaluation metrics, including, MAE, RMSE, MAPE, RMSRE, MARE, and PBIAS, to comprehensively assess their accuracy and reliability. The outcome of the present study provides valuable insights into the performance of different ML algorithms and suggests potential avenues for further research. This paper aims to address a critical gap in the existing literature by leveraging ML to predict the porosity of granite at elevated temperatures during different cooling treatments, ultimately contributing to the efficient and sustainable utilization of geothermal resources.

Experimental techniques

The Jalore granite samples used in our study were obtained from the Rajasthan province in India, which is located between latitudes 24°37′ and 25°49′ and longitudes 71°11′ and 73°05′ (Gautam et al. 2018a). These granite rock specimens have been categorized into three groups based on their grain size: fine-grained (FG), medium-grained (MG), and coarse-grained (CG). The categorization of the grain size is due to the mineralogical variation of granite, since finer grains offers a wider surface area for the propagation of induced thermal stress, while coarser grains have fewer grain boundaries and larger crystal diameters, leading to a unique distribution of thermal stress. Their distinctive microstructures, marked by larger mineral crystals, are less prone to rapid microcrack formation; yet, they may exhibit localized cracking due to uneven heat distribution or differential mineral expansion during thermal cycles. The granite samples were cut into 25-mm-diameter by 50-mm-long cylindrical specimens. The end face of the specimen was prepared to maintain parallelism within a tolerance of 0.3 mm, and the tangent planes were aligned to assure parallelism within a tolerance of 0.1 mm. To evaluate accuracy and repeatability, each test setup consists of two granitic specimens as shown in Fig. 1a, each containing fine, medium, and coarse grain granite samples, as observed in petrographic microscopic (Fig. 1b). All the specimens are soaked with water in a vacuum for one hour before any experimental research. They are then put into an oven and held at 105 °C for 24 h to eliminate all surface moisture. A muffle furnace was utilized to investigate the thermal properties of all granitic specimens undergone thermal treatment. The specimens were heated at a periodically elevated temperature with a regular interval of 25 °C starting from room temperature 25 °C to 1000 °C, maintaining a heating rate of 5 °C/min, as illustrated in Fig. 2. The thermocouple data recorder monitored the rock specimens to ensure they reached the target temperature and maintained it for the full 12 h. The uniform temperature gradients induced by this treatment method effectively mitigate the adverse effects of thermal shock, ensuring consistent and uniform thermal dispersion across all specimens. The specimens were subjected to heating followed by cooling using one of the two methods – FC and WC, to simulate the realistic natural geothermal treatments. The specimens were initially subjected to FC, wherein the furnace was turned off, and specimens were allowed to cool gradually (0.39 °C/min) to ambient temperature. Subsequently, another set of specimens were rapidly cooled via WC by submerging them into the water. The steep temperature gradient (137.48 °C/min) induced by WC causes the outer surficial layers of the rock to cool and contract more quickly than the inner layer, leading to high thermal stress and extensive microcracking and fracture formation.

The degree of cyclically induced damage is correlated with the cooling rate and the heating temperature, suggesting that fast temperature gradients formed throughout the sample could contribute to thermal damage (Bonazza et al. 2009; Zhou et al. 2018). Figure 2 illustrates jalore granite

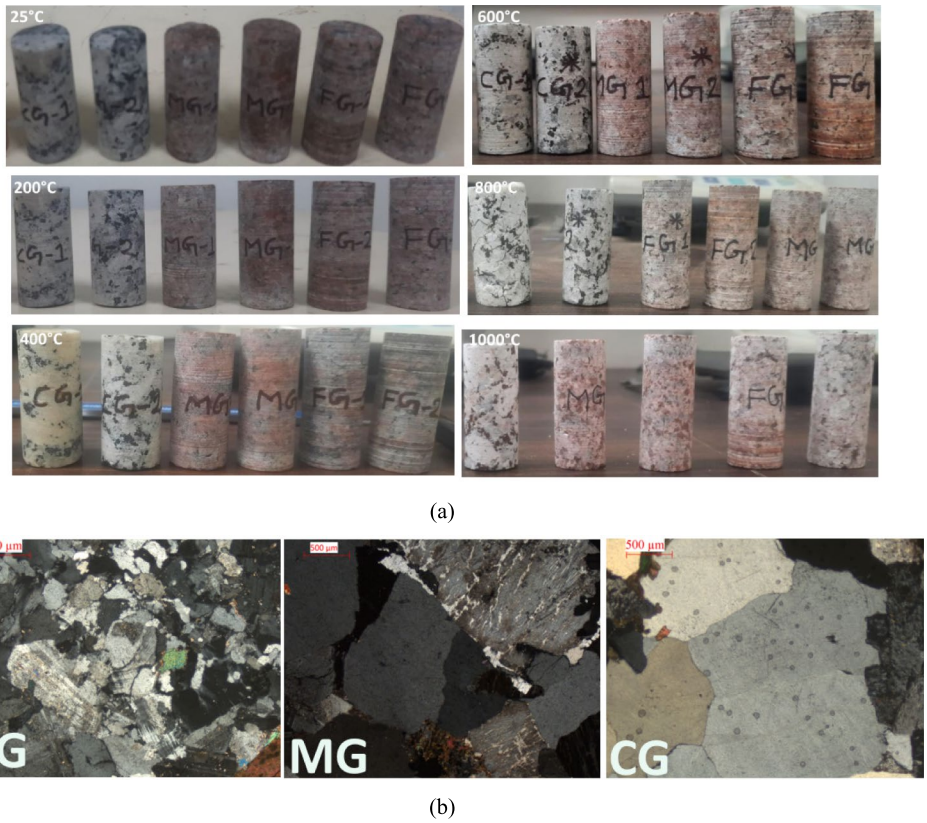

Fig. 1 Different types of heated granite specimens' appearance (**a**) 25°C, 200°C, 400°C, 600°C, 800°C, 1000°C (**b**) Petrographic microscope image of FG, MG and CG granite rock specimens at room temperature

specimens subjected to various heating and cooling treatments at different elevated temperatures.

The porosity of the samples was assessed utilizing an automatic gas pycnometer (PYC-100 A, PMI), as depicted in Fig. 3a. The instrument quantifies the volume of Helium (He) gas displaced by the sample, as He can enter even the finest pores enables precise measurements of volume. The precise measurement of volume is crucial for determining porosity. To ensure the reliability and reproducibility of the data, multiple measurements were conducted. The Olympus wave detector were used to measure P- and S-wave velocity as shown in Fig. 3b. Mount P-wave (500 kHz) and S-wave (1 MHz) transducers to the specimen surfaces, ensuring optimal contact between the transducers and the rock specimen by applying coupling gel. Measure and record the wave propagation through the specimen.

Machine learning methodologies

This section outlines the data exploration process and the techniques utilized for data preprocessing, followed by the training and validation of machine learning models. Finally, the predictive modeling methodology was used for evaluating rock porosity. Figure 4 shows the general workflow for predicting the porosity from the rock properties (temperature, mass, p-wave velocity, s-wave velocity, and grain type). After comprehensive data exploration and preprocessing of the data, six ML models—RF, XGBoost, SVM, KNN, Catboost, and LightGBM—were trained on the designated training datasets and subsequently validated on the test datasets using R^2 (R-squared) and multiple error metrics such as, RMSE, MAE, MAPE, RMSRE, MARE, and PBIAS.

Data exploration

Exploratory Data Analysis (EDA) represents a fundamental phase in the machine learning pipeline, facilitating a comprehensive understanding of the data set by identifying underlying patterns, detecting anomalies, and allowing preliminary hypotheses testing. The datasets used were divided into two sets: the furnace-cooled dataset and the water-cooled dataset, presenting a variety of statistics that aid in formulating robust hypotheses for model training and inference.

Present datasets also include the grain type as one property. We consider 3 categories of grains: fine grain, medium grain, and coarse grain. The data comprise 40 records of fine grains and medium grains each and 36 records for coarse-grained, accounting for a total of 232 records for both data

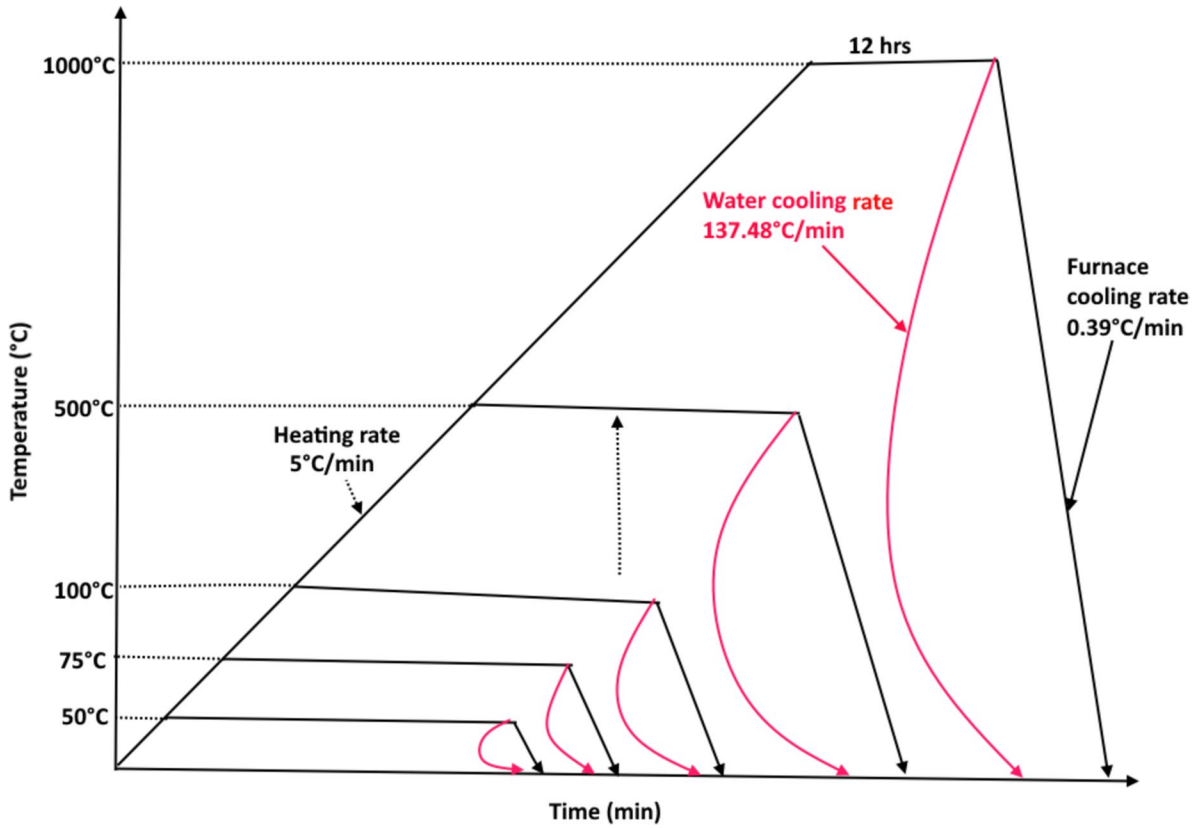

Fig. 2 The testing protocol involves heating and cooling specimens using a furnace and water

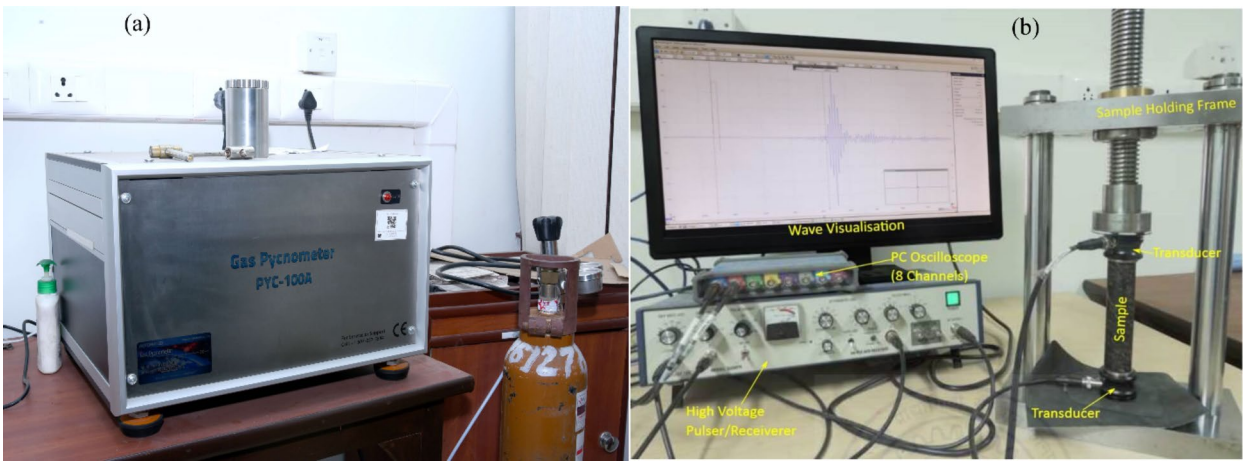

Fig. 3 Evaluation of porosity and acoustic wave velocity (**a**) Gas Pycnometer (**b**) Experimental setup for measuring P-wave and S-wave velocities

sets corresponding to two kind of cooling methods FC and WC in present study, as shown in Tables 1 and 2.

The temperature variable is consistent across both categories, ranging from 25 °C to 1000 °C, with a mean value of approximately 497 °C and a standard deviation of 282 °C. This uniformity ensures that any differences in other parameters are due to the cooling method rather than variations in temperature treatment.

For mass, rock specimens cooled in water have a slightly higher mean mass (40.31 g) compared to those cooled in a furnace (40.06 g), with respective standard deviations of 2.80 g and 2.30 g. The water-cooled rock specimens exhibit

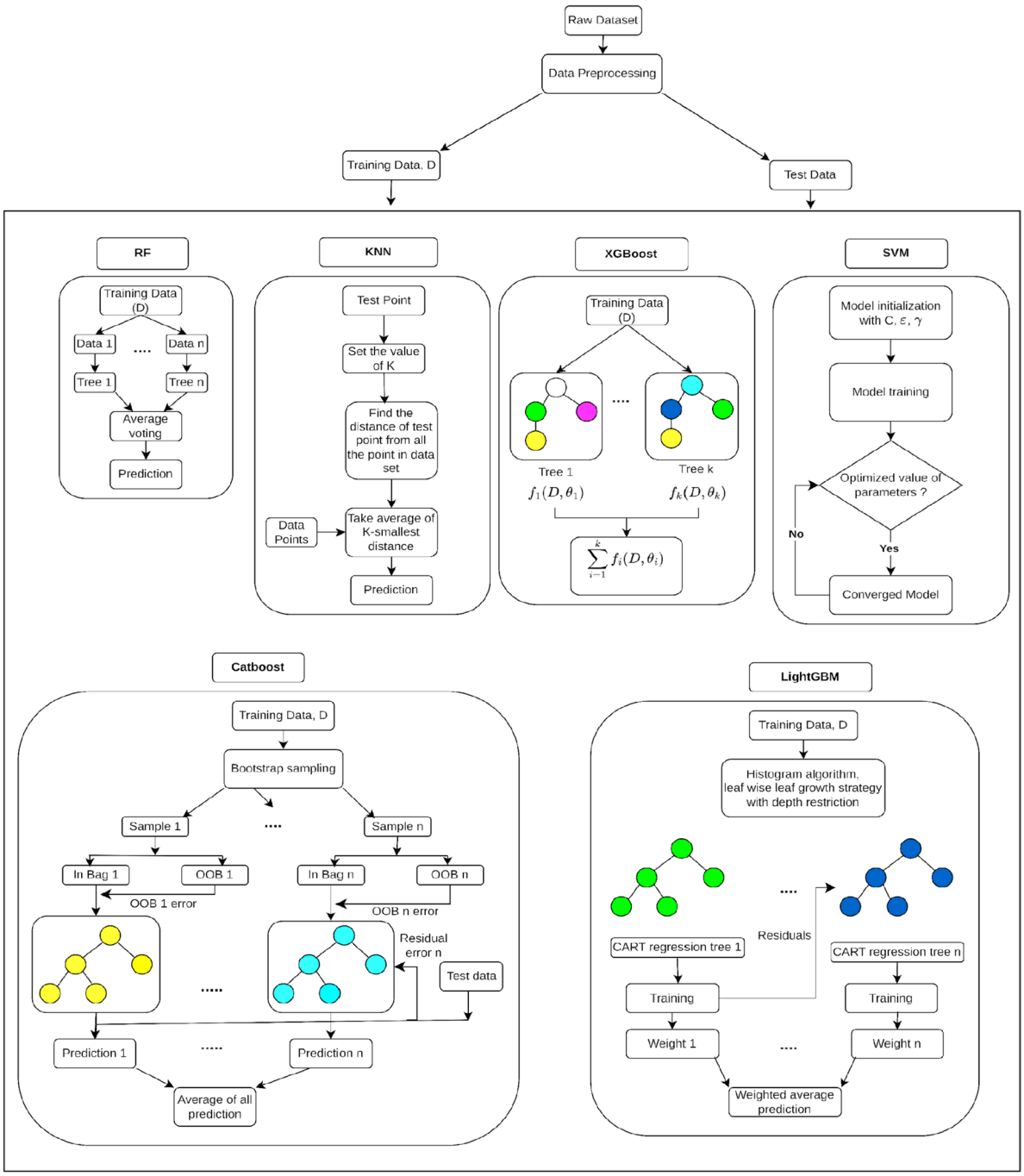

Fig. 4 Flowchart of working of different Machine learning models

a wider range of mass, as indicated by the higher standard deviation.

The p-wave velocity and s-wave velocity also show notable differences. The mean p-wave velocity for water-cooled rock specimens is slightly lower (2.86 km/s) compared to furnace-cooled rock specimens (2.93 km/s), with similar standard deviations around 1.78–1.79 km/s. The s-wave velocity is marginally higher for water-cooled rock specimens (1.68 km/s) than for furnace-cooled ones (1.66 km/s), with a slightly lower standard deviation in the former.

Porosity presents the most significant difference between the two categories. Water-cooled rock specimens have a higher mean porosity (4.28%) compared to furnace-cooled rock specimens (3.19%), with higher variability (standard deviations of 2.59% vs. 2.37%). The higher maximum porosity in water-cooled rock specimens (11.13%) compared to

furnace-cooled rock specimens (10.86%) further emphasizes this disparity.

The correlation heatmap (Fig. 5) for both the furnace-cooled and water-cooled categories provides insights into the linear relationships between the variables (temperature, mass, p-wave velocity, s-wave velocity, and porosity). The correlation matrix (heatmap) for furnace cooled specimens shows strong negative correlations between temperature and

Table 1 Descriptive Statistics of Thermally Treated Rocks with furnace cooling

Statistic	Temperature (°C)	Mass (g)	*P* wave velocity (km/s)	S wave velocity (km/s)	Porosity (%)
Count	116	116	116	116	116
Mean	496.98	40.06	2.93	1.66	3.19
Std Dev	282.11	2.30	1.78	1.06	2.37
Min	25.00	36.00	0.36	0.21	0.07
25th Percentile	250.00	38.41	1.11	0.57	1.32
Median (50th Percentile)	500.00	38.91	3.08	1.64	3.10
75th Percentile	731.25	43.01	4.46	2.66	4.14
Max	1000.00	43.30	5.78	3.54	10.86

Table 2 Descriptive Statistics of Thermally Treated Rocks with Water cooling

Statistic	Temperature (°C)	Mass (g)	*P* wave velocity (km/s)	S wave velocity (km/s)	Porosity (%)
Count	116	116	116	116	116
Mean	496.98	40.31	2.86	1.68	4.28
Std Dev	282.11	2.80	1.79	1.00	2.59
Min	25.00	37.50	0.38	0.23	0.36
25th Percentile	250.00	38.12	1.17	0.70	2.33
Median (50th Percentile)	500.00	38.90	2.60	1.60	3.87
75th Percentile	731.25	44.10	4.62	2.59	5.42
Max	1000.00	44.20	6.11	3.25	11.13

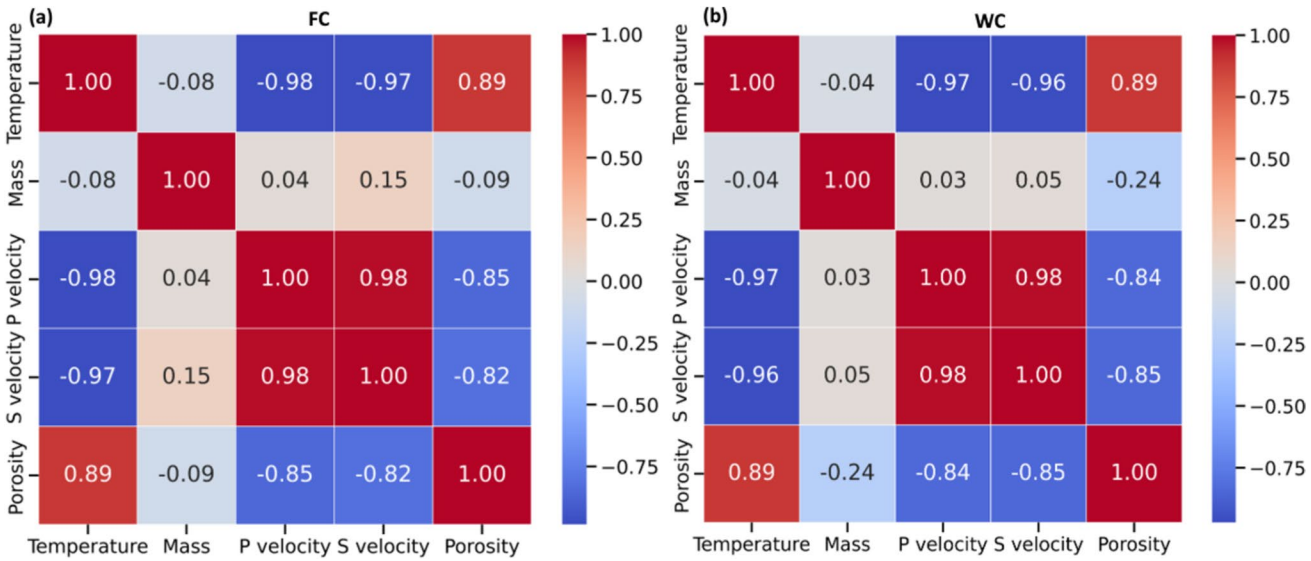

Fig. 5 Correlation Heatmap for (**a**) furnace cooling and (**b**) water cooling

both p-wave velocity ($r = -0.98$) and s-wave velocity ($r = -0.97$), indicating that as the temperature increases, the velocities of both waves decrease. Additionally, there is a strong positive correlation between temperature and porosity ($r = 0.89$), suggesting that higher temperatures lead to increased porosity. The weak correlations between mass and the other variables indicate that mass does not significantly influence or is influenced by the other parameters in the context of furnace cooling.

The correlation matrix for water cooled specimens demonstrates similar patterns to those observed in furnace cooled specimens, showing strong negative correlations between temperature and both p-wave velocity ($r = -0.97$) and s-wave velocity ($r = -0.96$), as well as a strong positive correlation between temperature and porosity ($r = 0.89$). Notably, the correlation between mass and porosity is slightly weaker ($r = -0.24$) in water cooled specimens compared to furnace cooled ones, suggesting a subtle yet significant relationship. The pair plot effectively visualizes these relationships between variables while simultaneously illustrating the distribution of each individual variable, providing a comprehensive view of the dataset's structure and interdependencies, as depicted in Fig. 6(a & b).

The pair plots for furnace-cooling and water-cooling effect visually reinforces the insights gained from the correlation matrix. The scatter plots demonstrate the strong negative linear relationships between temperature and the velocities, as well as strong positive linear relationship between temperature and porosity. The diagonal plots show the distribution of each variable, where temperature, and porosity shows a normally distribution curve,

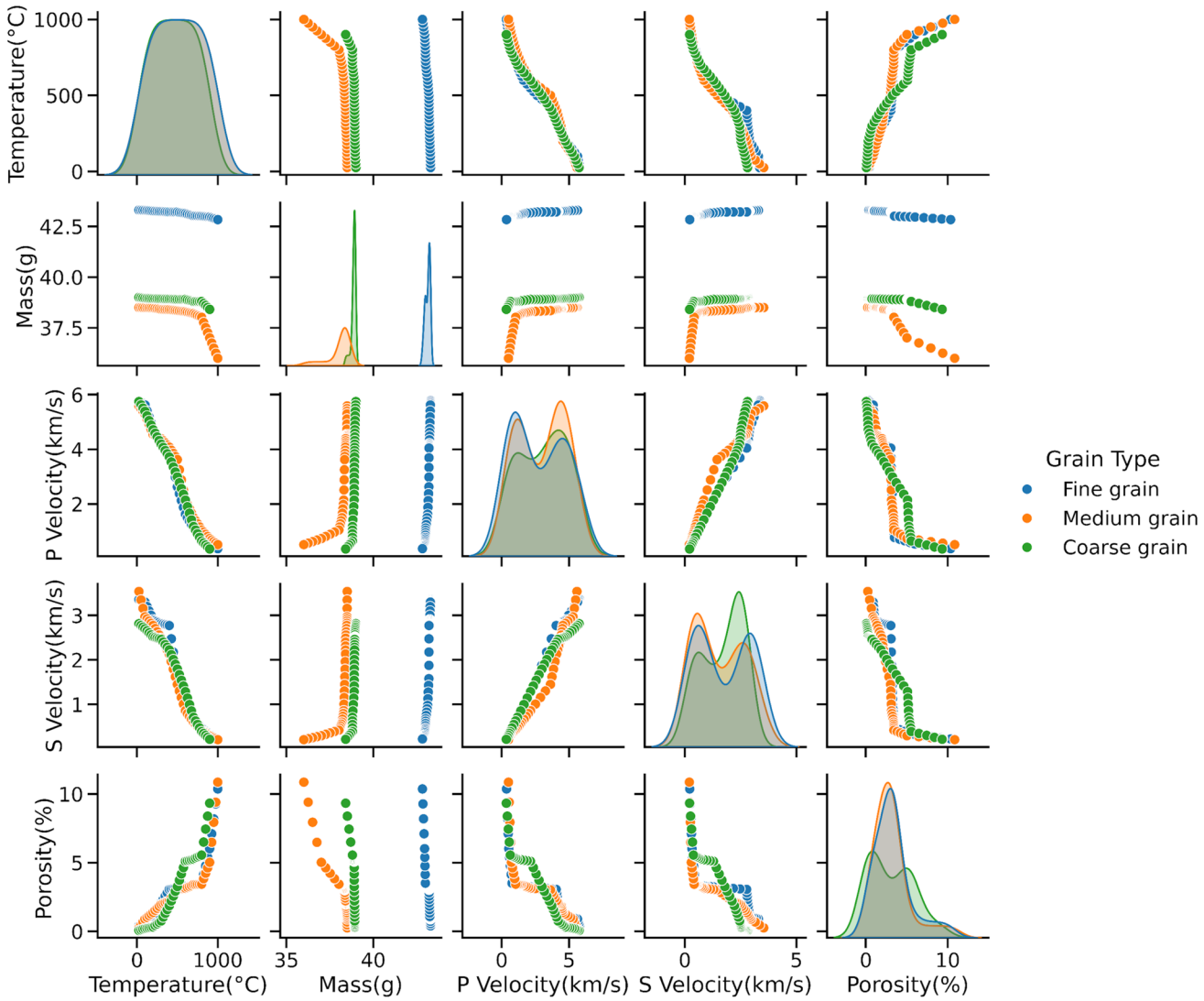

Fig. 6 (**a**) Pair plots for thermally treated and furnace-cooled granite rock specimens. (**b**) Pair plots for thermally treated and water-cooled granite rock specimens

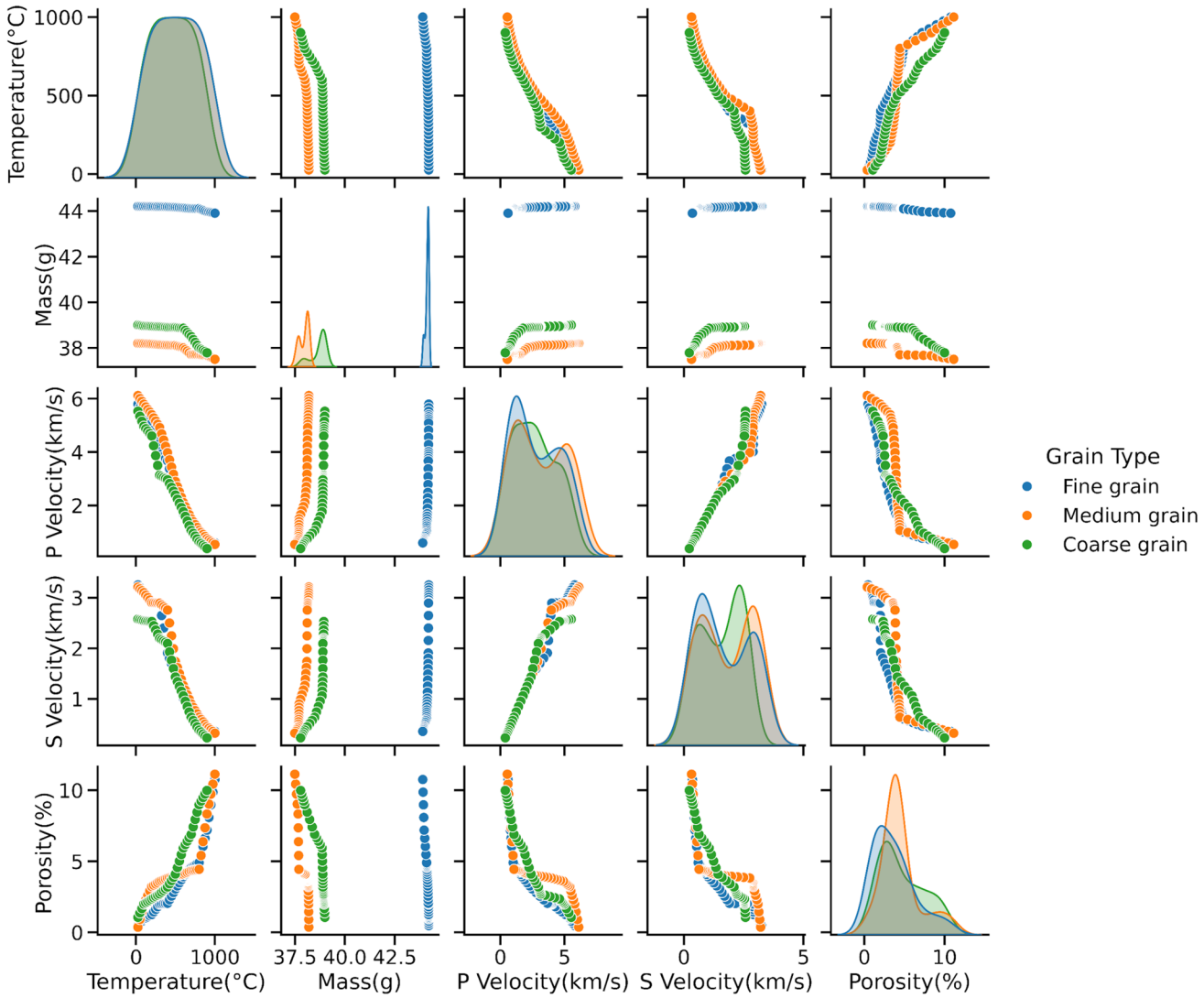

Fig. 6 (continued)

while mass shows a consistent plot having less variability and p-wave and s-wave velocity shows a bi-modal shape of their distribution.

These analyses suggest that temperature affects physical properties of thermally treated rocks, reducing wave velocities and increasing porosity after heating-cooling treatment for both furnace-cooled and water-cooled rock specimens. The relatively consistent value of mass demonstrate that mass is less influenced by thermal treatment compared to other properties.

To further visualize our data distribution and their statistical characteristics for each grain type category, two different types of plots, including violin plots and box plots, are depicted in Fig. 7. These plots represent porosity data for two different cooling methods: FC and WC. The comparisons are classified into fine, medium, and coarse grains. A simplified analysis and comparison, along with the behavior of rocks during various cooling processes, are outlined below:

The box plots (Fig. 7a&b) illustrate the diversity in porosity, including the median, interquartile range (IQR), and outliers. The median porosity for the furnace-cooled rock specimens is around 3.5%, with maximum values under 3.8%, while for the water-cooled ones, it is around 3%, having a symmetric distribution around the median and occasional values exceeding the upper quartile (5.8%). The range of porosity values in furnace-cooled rock specimens for fine grain is smaller than the water-cooled counterparts. We left some data points which are beyond Q3 + 1.5 * IQR (interquartile range) and below Q1–1.5 * IQR, as they represent natural variation in our dataset and do not stem from measurement or processing errors. Porosity generally increases in furnace-cooled rock specimens from fine to coarse grain, and coarse grain specimens show maximum porosity values

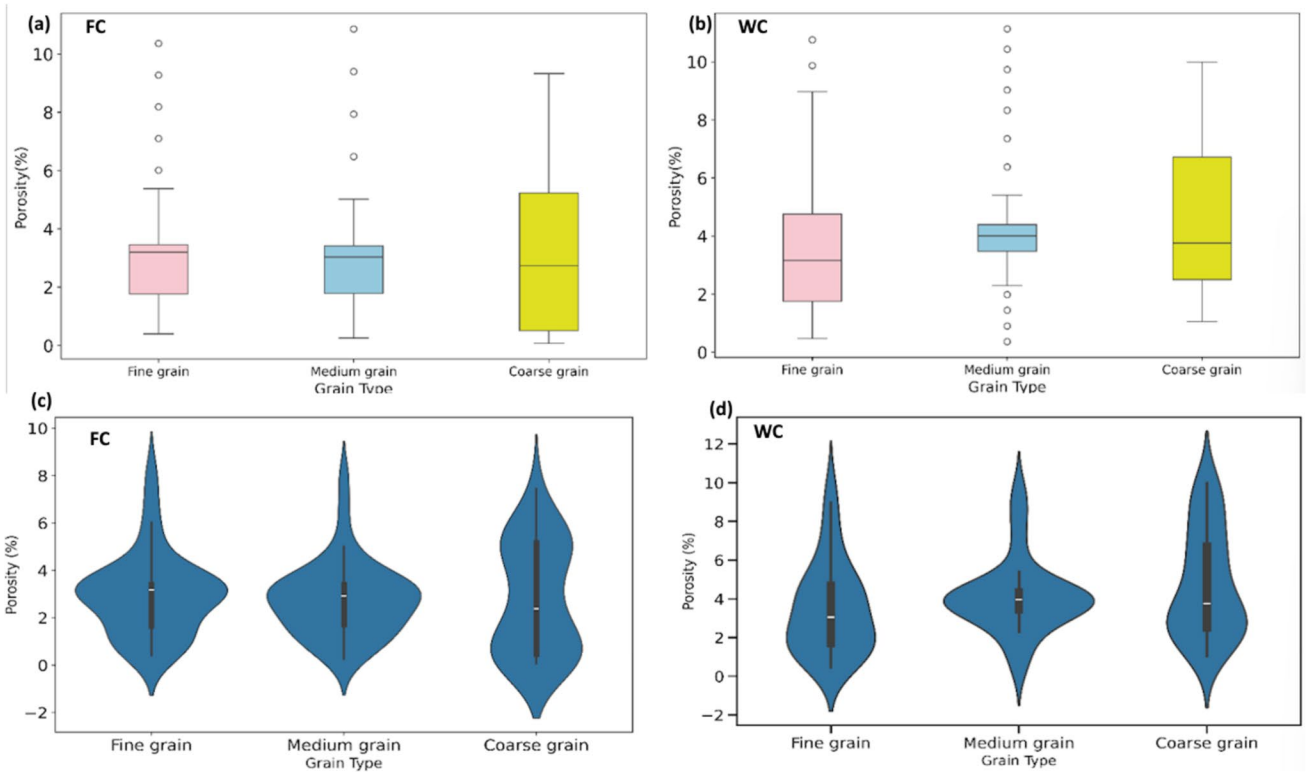

Fig. 7 Boxplots and Violin plots for furnace cooled and water-cooled rock specimen

and higher variability. Water cooled rock specimens also depict a similar pattern, but illustrate relatively higher porosity for all grain types. Furnace-cooled rock specimens yield much better uniformity in porosity, and even coarser grains maintain relatively stable crystalline structures despite very high porosity. In contrast, rock specimens quenched by WC, are more heterogeneous, as even fine-grain specimens are quite vulnerable due to structural defects produced by rapid cooling.

The violin plots (Fig. 7c&d) show characteristic porosity distributions for three grain sizes subjected to FC and WC conditions, with pronounced differences in morphology. The values of porosity in both cooling methods are predominantly in the range.

of 0–10% for FC and 0–12% for WC, with the highest number of observations in the range of 2–4%. The data is found to exhibit asymmetric bimodal distributions for all grain types, indicating two prevalent porosity regimes. A more distinct separation between modes is seen for water cooled rock specimens, specially coarse grain specimens are illustrating more pronounced bimodal distribution. Fine grains maintain the narrowest distribution spread in both cooling methods, which indicates a uniform pore formation in relatively stable microstructure. Water cooled rock specimens tend towards somewhat higher maximum porosities as well as broader distributions, specially in the coarse grain size range, suggesting that the quenched rapid cooling induces considerable thermal stress, leading to increased porosity variability and structural instability. Furnace cooled rock specimen is cooled gradually, depicting more homogeneous and regular grain structures than those of water-cooled specimens.

Data preprocessing

Data preprocessing has its own place in ML pipeline and is used to transform raw data into suitable format for model training. The key part of this process is cleaning, transforming and organizing data to make the model more reliable and robust to perform much better. The real-world datasets are mostly imperfect and inconsistent; thus, data preprocessing is essential to overcome issues such as missing values, the presence of noise, and disparity in scales. Efficient data preprocessing can significantly enhance the efficiency and accuracy of ML models. In this study, the first primary data preprocessing step was ‘one hot encoding’, applied to the grain type, which is categorical data. Categorical data is where there are distinct categories or labels, and the ML algorithms usually require numerical input. One hot encoding transforms these grain type data into a favourable ML format in order to improve its prediction performance. For example, if our grain type data contains three categories:

fine, medium, and coarse, these will be converted into three binary columns, each representing whether a category is present or absent. This preprocessing process also prevents the ML models from assuming any ordinal relationship between the categories to preserve the integrity of categorical data. Furthermore, in order to induce natural variability in our data, we added Gaussian noise to each rock property. We added noise to 5% of the standard deviation of each feature. Gaussian noise is characterized by its normal distribution; it is commonly added to data to simulate real-world variations and prevent the model from overfitting. The Gaussian noise is defined by Eq. 1, which is characterized by mean μ and variance σ^2

$$p(z) = \frac{1}{\sigma\sqrt{2\pi}} e^{\frac{-(z-\mu)^2}{2\sigma^2}} \quad (1)$$

Overfitting occurs when a model captures the noise and spurious details in the training data to the extent that it negatively impacts the performance on unseen new datasets. Therefore, the incorporation of controlled noise to training processes enables the ML models to generalize effectively to unseen new datasets and have high generalization capacity. The 5% noise is chosen to maintain a balance by introducing variability without distorting underlying data distribution. The data scaling transformation was performed after noise addition. Data scaling is required as ML algorithms in general, specially those involving gradient descent optimization, are sensitive to scales of the features. Variations in feature sizes may cause specific variables to disproportionately affect the training process of the model, perhaps resulting in suboptimal performance. Data scaling makes sure that all the input features contribute in a proper proportion so that model doesn't lose its numerical stability and also can improve it converges efficiency during optimization. Generally, data scaling include standardization, which adjust the data to have a mean of 0 and a variance of 1, and normalization, which scales the data to a range between 0 and 1. As such, this study used a standardization technique that normalized the feature distributions such that all input features were uniform and consistent.

Machine learning models and training approach

In this section, a complete methodology is described to select, train, validate and assess various ML models for predicting granite porosity under elevated temperatures followed by FC and WC. Six ML models were employed in this particular study: Random Forest (RF), Extreme Gradient Boosting (XGBoost), K-Nearest Neighbors (KNN), Support Vector Machine (SVM), Categorical Boosting (CatBoost), and Light Gradient-Boosting Machine (LightGBM). Each model has several hyperparameters that need tuning to achieve the best performance. The models were tuned for optimal performance using cross validation. Each model has several hyperparameters that need tuning to achieve the best performance. In this study, hyperparameter tuning in conjunction with k-fold cross-validation was used in order to optimize the performance of the used ML models in predicting the porosity of thermally treated granite (Fig. 8).

In order to find out the ideal hyperparameter settings for each model a comprehensive grid search has been conducted. The dataset was partitioned into training and testing sub-datasets, with 75% assigned for training and 25% used for testing. The partition was performed using the scikit-learn library, with a random state seed set for reproducibility of the result. This rigorous approach guarantees that the used ML models are to be well fitted and to be generalizable to unseen data, an essential prerequisite for reliable prediction. Each model has its own unique hyperparameters that significantly influence their performance. A comprehensive grid search with 5-fold cross-validation was implemented

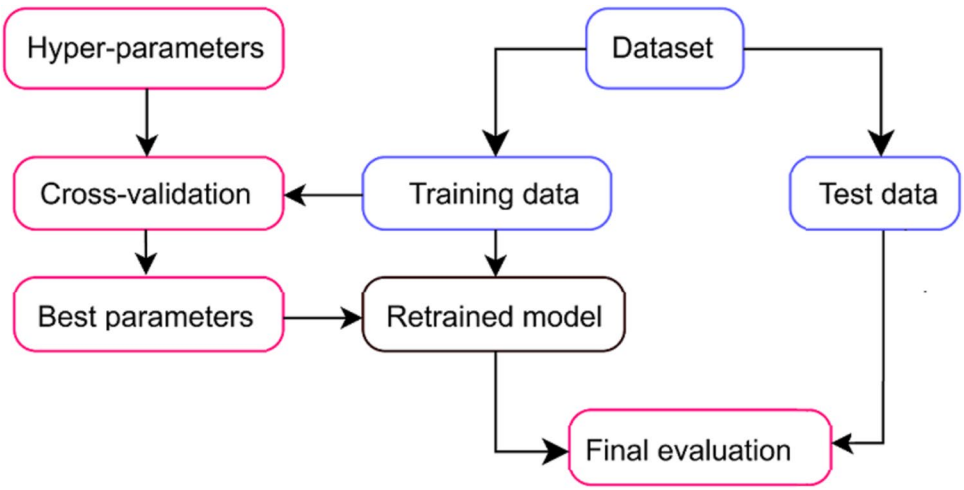

Fig. 8 Model training and evaluation flowchart

for hyperparameter tuning across all machine learning models. To determine the optimal set of hyperparameters, an exhaustive grid search was performed in combination with 5-fold cross-validation. This method divides the dataset into five distinct subsets, utilizing a cross-validation technique in which the model is trained on four subsets and assessed on the fifth. This process is performed iteratively to ensure that each subset functions as the validation set precisely once. The hyperparameters optimized for each model throughout this process are specified as follows:

- The hyperparameter search included several settings for various ML models. For tree-based models (RF, XGBoost, LightGBM), we tested the number of estimators (50–200) and the maximum tree depth (3–9). For SVM, we analyzed several values for the regularization parameter C (ranging from 0.1 to 10), different kernel types (radial basis function and polynomial), and gamma configurations ('scale' or 'auto'). We optimized the neighbor count (from 3 to 9) and the weighting mechanism utilized for distance calculation in K-Nearest Neighbors (KNN). We improved the number of iterations (100–300), tree depth (3–7), and learning rate (0.01–0.2) for gradient boosting models (CatBoost, LightGBM).
- The ideal configurations demonstrated a preference for moderate tree depths (5–7), a higher number of estimators (about 200), and learning rates ranging from 0.1 to 0.2. In SVM, the choice of kernel varied according to the task: a polynomial kernel was more effective for furnace data, while a radial basis function kernel was preferred for water cooling.

Results and discussion

The thermal and physical properties of fine, medium, and coarse-grained granite exposed to high elevated temperatures significantly depend on the cooling method. With gradual temperature reduction, FC tends to preserve the structural integrity of the rock and consequently cause minor variation in density, porosity, permeability, thermal expansion, and wave velocities. Conversely, the rapid cooling during WC, induces large thermal stresses from differential thermal expansion of the constituting minerals, which in turn results in extensive microcracking, reduced wave velocities and elevated porosity. These changes are also depending on the grain size of the granite, with coarse-grained granite more susceptible to thermal stress effects than fine and medium-grained granite.

The mineral composition of granite also significantly affects its thermal behavior. The dehydration of some hydrated minerals such as feldspar and micas at high temperature leads to mass loss. Granite contains quartz undergoes an alpha-beta phase transition at around 573 °C; this induces the internal stresses and microcracking, particularly during quenching.

As the temperatures reaches at around 400 °C, the intergranular microcracks slowly propagate and new intergranular microcracks are created by the thermal expansion mismatch of constituting minerals. Microcracks inside mineral grains become discernible at a temperature of 400 °C. As the temperature rises, intergranular and intergranular microcracks gradually propagate and coalesce, leading to the formation of macrocracks at 600 °C. After reaching a temperature of 800 °C, these macrocracks on the surface of coarse granite further expands and merge to form surface cracks. However, there is a significant influence of the cooling on development of granite surficial cracks. In granite, the progress of thermal damage under gradual FC is less severe than under rapid WC, illustrating the effect of cooling rate on the progression of thermal damage.

The prediction of porosity in thermally stressed rock specimens for both FC and WC conditions was performed using six ML regression models: RF, XGBoost, SVM, KNN, CatBoost and LightGBM. The efficacy of the all the used models were evaluated based on their performance during training, validation and testing phases.

Hyperparameter optimization was performed for each of the six regression ML methods to improve the accuracy of the models and their generalization abilities. In order to explore the parameter space, a systematic search methodology and k-fold cross validation were utilized, which enabled the determination of optimal hyperparameters for each model, leading to greater resilience to overfitting.

The performance differences noticed among the ML models is due to the inherent properties of granite and the mechanics controlling thermal stress and cracking. The thermal behavior of granite and its damage behaviour during thermal treatments is significantly governed by the mineral composition, grain size, and the mismatch of thermal expansion coefficient among minerals.

Furnace cooling

The results for the furnace cooled rock specimens demonstrate that the fine-tuning hyperparameters and k-fold cross-validation significantly enhance the performance of ML models. All the six tested ML models demonstrate varying degree of accuracy and reliability, with each model assessed using multiple error metrics. Among all the six tested ML methods, the CatBoost regressor methods outperform others, yield the highest accuracy with an R-squared value 0.994 and lowest errors with RMSE (0.138), MAE (0.104), and MAPE (0.154) values on the test set as depicted in Fig. 9. These findings emphasize the applicability and performance

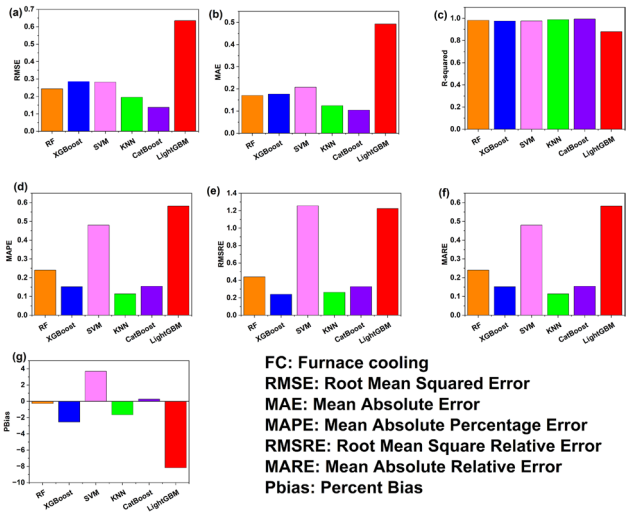

Fig. 9 Models performance for furnace cooling (**a**) RMSE, (**b**) MAE, (**c**) R-Square, (**d**) MAPE, (**e**) RMSRE, (**f**) MARE, (**g**) PBIAS

assessment of utilized ML models in predicting the porosity of granite under various cooling conditions are obtained.

RF exhibits robust performance with an R-squared value of 0.982 and error metrics such as an RMSE of 0.244, MAE of 0.171, and MAPE of 0.240, capturing most of the data variance. The ensemble nature of RF, which combines multiple decision trees, effectively model complex non-linear relationships, making it suitable for predicting porosity variation induced by thermal treatment of rock specimens. PBIAS is also negligible (−0.269), showing minimal bias. XGBoost also does relatively well with R-squared (0.976) and RMSE (0.285), MAE (0.177), MAPE (0.152). Its gradient boosting framework which sequentially corrects errors from preceding trees, making is particularly effective in capturing the complexities of variation in porosity of rock specimens at different temperatures. However, negative PBIAS (−2.541) signifying a slight underestimation. SVM shows slightly higher errors, with the RMSE of 0.282, MAE of 0.208, MAPE of 0.480 and shows decent accuracy with an R-squared value of 0.976. This model is quite sensitive to parameter tuning and multi- dimensionality of the data, which limits its performance. Despite its proven efficacy in classification, the performance of SVM used for regression tasks significantly relies on the choice of kernel function and regularization parameters, which may limit its regression performance. A moderately positive PBIAS (3.683) indicates a tendency to overestimation.

KNN performs exceptionally well, attaining a high accuracy with an R-squared value of 0.989 and lower error metrics value such as an RMSE of 0.195, MAE of 0.208, MAPE of 0.114. Its superior ability to utilize the similarity of proximal data points, making it effective in predicting granite porosity. This characteristic is particularly useful in studying the localized data patterns such as grain size and thermal stress in granite rock. PBIAS (−1.658) reflects minimal bias. CatBoost outperforms all models, attaining highest accuracy with an R-squared value of 0.994 and lowest error metrics such as RMSE (0.138), MAE (0.104), and MAPE (0.154). Its use of ordered boosting and handling of categorical features enables it to precisely identifies complex variations in porosity of rock specimens exposed to thermal treatments. Its strong performance demonstrates its suitability for high precision modeling tasks requiring thermally treated material characteristics. The low PBIAS (−0.265) shows minimal bias.

LightGBM shows comparatively lower prediction accuracy with an R-squared value of 0.879, and evidenced by an error metrics such as RMSE of 0.635, MAE of 0.493 and MAPE of 0.58. Although LightGBM is well known for quick and robust processing of large datasets, it finds it challenging to manage the complex variation in rock properties during thermal heating and cooling processes. The comparatively higher error values showed that LightGBM may not be as suitable for this particular application. A significant underestimation is reflected by PBIAS (−8.172).

Scatter plots comparing True vs. Predicted datasets value for six ML models - RF, XGBoost, SVM, KNN, CatBoost, and LightGBM is illustrated in Fig. 10. This comparison among the all six used ML models reveals varying levels of predictive accuracy. The predictive performance for RF, XGBoost, and CatBoost ML methods are exceptionally well, as the data points closely aligning along the reference diagonal line for both training and testing datasets, indicating high accuracy and negligible overfitting. KNN and LightGBM perform moderately well, but minor deviations at higher values suggest limited generalization to extreme data points. The dispersion of data points for SVM model is significant specially for larger values that may indicate its difficulties in modeling the data non linearity.

Residual analysis of data points, as illustrated in Fig. 11; provides more insights into model's performance and the error characteristics. CatBoost has the most compact residual distribution and minimal error variability, making it most accurate model. However, the residual distribution for LightGBM has a wider and more irregular residual spread, with significant skewness and deviations, indicating challenges in accurately predicting porosity for coarse-grained rock. RF and XGBoost demonstrate nearly symmetric distributions centered around zero, characterized by a smaller range of residuals, indicating robust performance and low bias. SVM and KNN demonstrate marginally broader distributions, probably due to difficulties in managing the non-linear correlations and heterogeneity linked to coarse-grained samples, where porosity variations are more evident. SVM shows a small positive skewness in its residual, whereas, KNN residuals clustering around zero with higher variance.

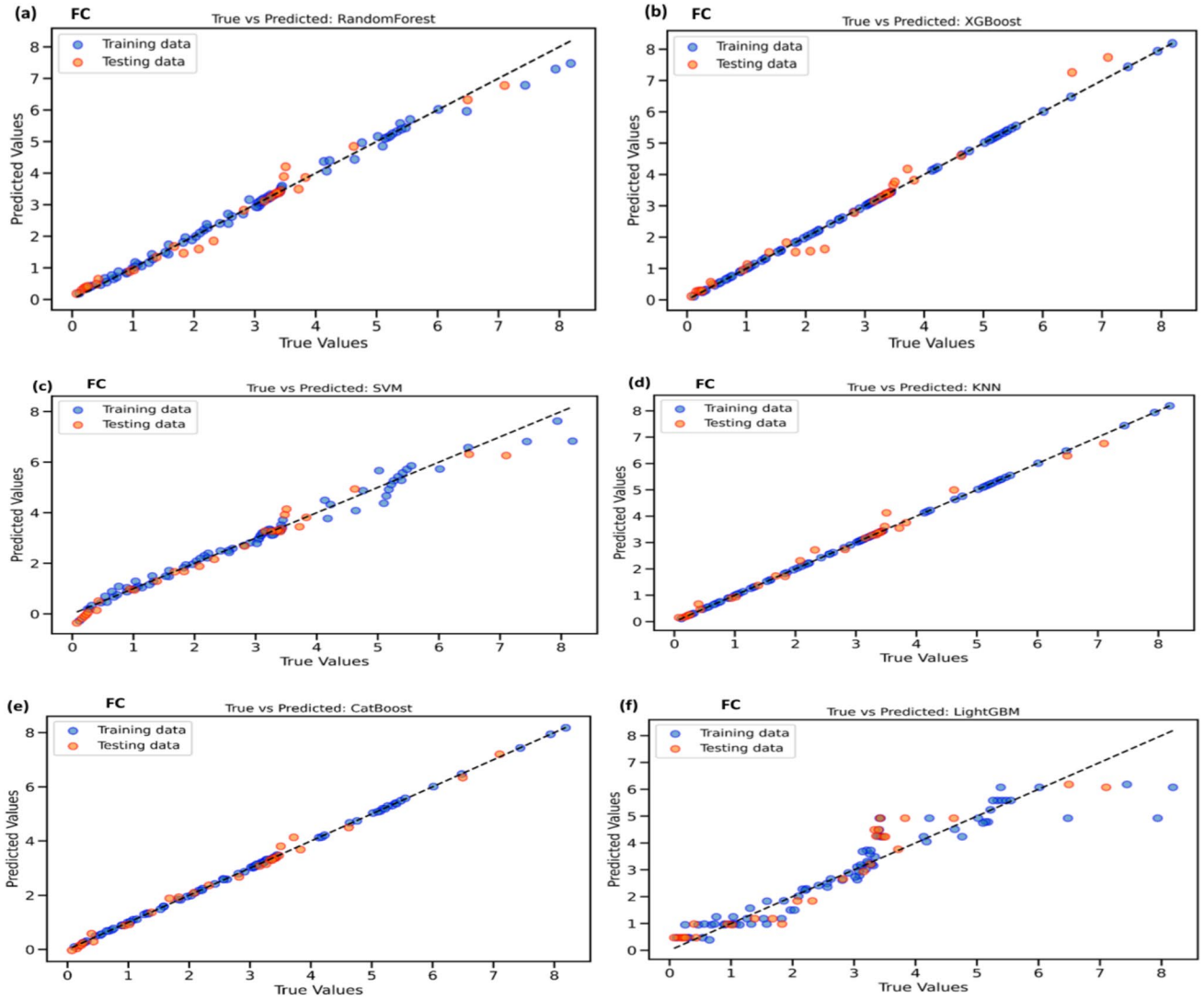

Fig. 10 True vs. Predicted scatter plots for FC across six ML models (**a**) RF, (**b**) XGBoost, (**c**) SVM, (**d**) KNN, (**e**) CatBoost, (**f**) LightGBM

It was found that, overall, CatBoost and RF exhibit excellent performance in minimizing residual and errors, showing higher predictive accuracy than other models.

Water cooling

The results for the water-cooled rock specimens reveals the CatBoost regressor ML model achieved the highest predictive performance for thermally treated granite rock specimens, as evidenced by the highest R-squared value 0.994 and the lowest RMSE (0.198), MAE (0.122), MAPE (0.059) on the test set, as illustrated in Fig. 12. The ability of CatBoost model demonstrates that it is very efficient at predicting the porosity, specially during fast cooling events. It is clearly evidenced by its ability to reduce both absolute and relative errors, shown by its low MAPE (0.0589) and RMSRE (0.167).

RF model maintains a robust predictive performance, with an R-squared of 0.984 and low errors such as (RMSE: 0.317, MAE: 0.258, and MAPE: 0.085) and minimal bias (PBIAS: −1.116), as illustrated in Fig. 12. The consistent performance of RF under different cooling conditions highlights its reliability and the superior generalization capability. XGBoost also performs very well, with an R-squared of 0.978 and moderate errors (RMSE: 0.363, MAE: 0.272, and MAPE: 0.084). However, its PBIAS value (−4.0392) shows a moderate underestimation. These characteristics of XGBoost shows that it is competitive, but slightly less than both RF and CatBoost. The SVM model yield less reliable prediction accuracy, achieving an R-squared value of 0.950 and higher error metrics (RMSE: 0.551, MAE: 0.340, and MAPE: 0.108). It was found that it can be more predictive with additional hyperparameter optimization or implementing new appropriate kernel functions. PBIAS (−4.31951)

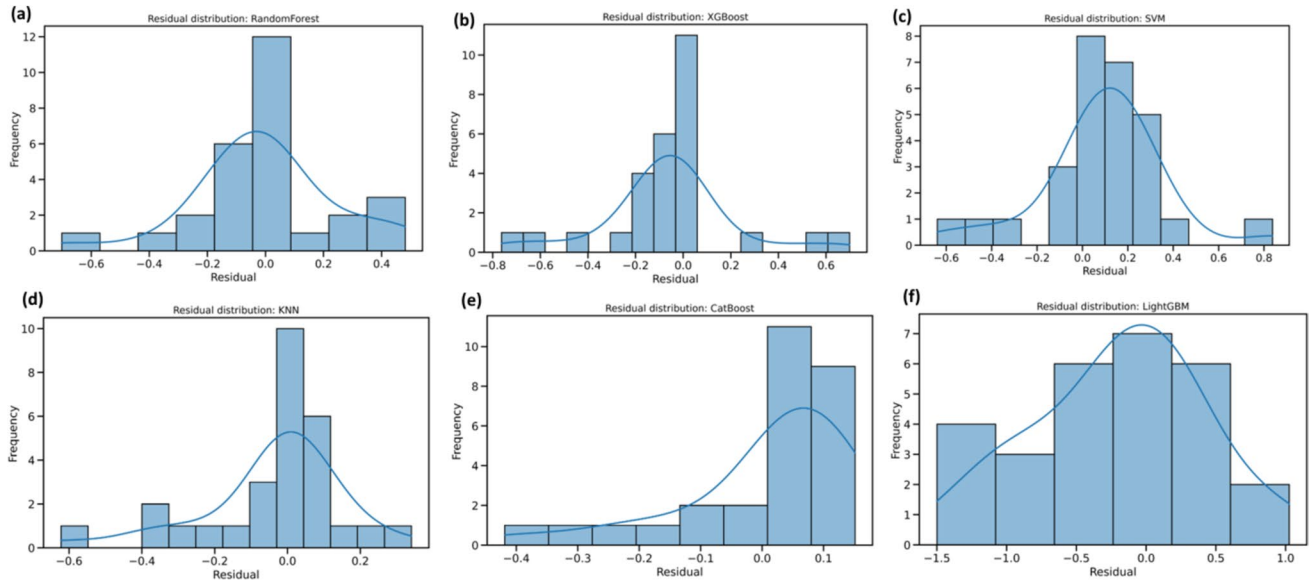

Fig. 11 Residual distribution for FC across six ML models (**a**) RF, (**b**) XGBoost, (**c**) SVM, (**d**) KNN, (**e**) CatBoost, (**f**) LightGBM

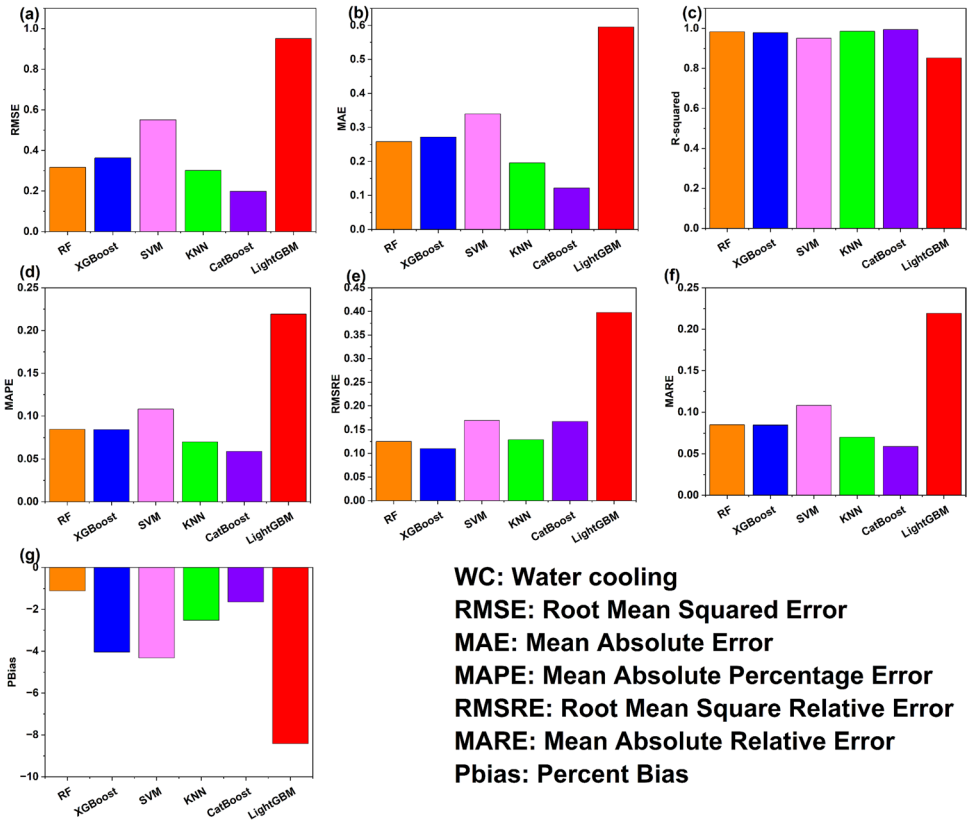

Fig. 12 Models performance for water cooling (**a**) RMSE, (**b**) MAE, (**c**) R-Square, (**d**) MAPE, (**e**) RMSRE, (**f**) MARE, (**g**) PBIAS

indicates a considerable bias, which further reduces its efficacy.

The KNN performs tremendously well with accuracy of 0.985 with R squared, and low error (RMSE: 0.301, MAE: 0.196, and MAPE: 0.070). Its nearest neighbor approach more closely depicts localized thermal stress and fractures arising from rapid cooling. A low PBIAS (−2.525) reflects minimal bias. CatBoost stands out as the best ML model,

achieving the highest R-squared value of 0.994 and the lowest errors (RMSE: 0.198, MAE: 0.122, and MAPE: 0.059). The remarkable ability of CatBoost to precisely find the complex correlations and non-linear pattern within the dataset with minimal bias PBIAS (−1.646), shows its reliability and precision.

In contrast, LightGBM model shows a suboptimal performance, with the lowest R-squared value of 0.852 and highest errors (RMSE: 0.951, MAE: 0.595 and MAPE: 0.219). Additionally, a large PBIAS (−8.412) indicates a significant underestimation.

To evaluate the predictive performance of the six ML models- RF, XGBoost, SVM, KNN, CatBoost, and LightGBM—a comparison of True vs. Predicted values was made using scatter plots, as illustrated in Fig. 13. The training and testing data points are closely align with the reference diagonal line, indicating strong predictive accuracy and minimal overfitting. Among all six used ML models; RF, XGBoost, and CatBoost demonstrate superior accuracy, with closely matched data points. While KNN performed comparably well, the testing dataset shows slight errors at higher values, because of some irregularities the testing dataset. SVM model showed greater dispersion, specially for larger values. It reveals its difficulty in exactly capturing complex data patterns causing a degree of underfitting. LightGBM

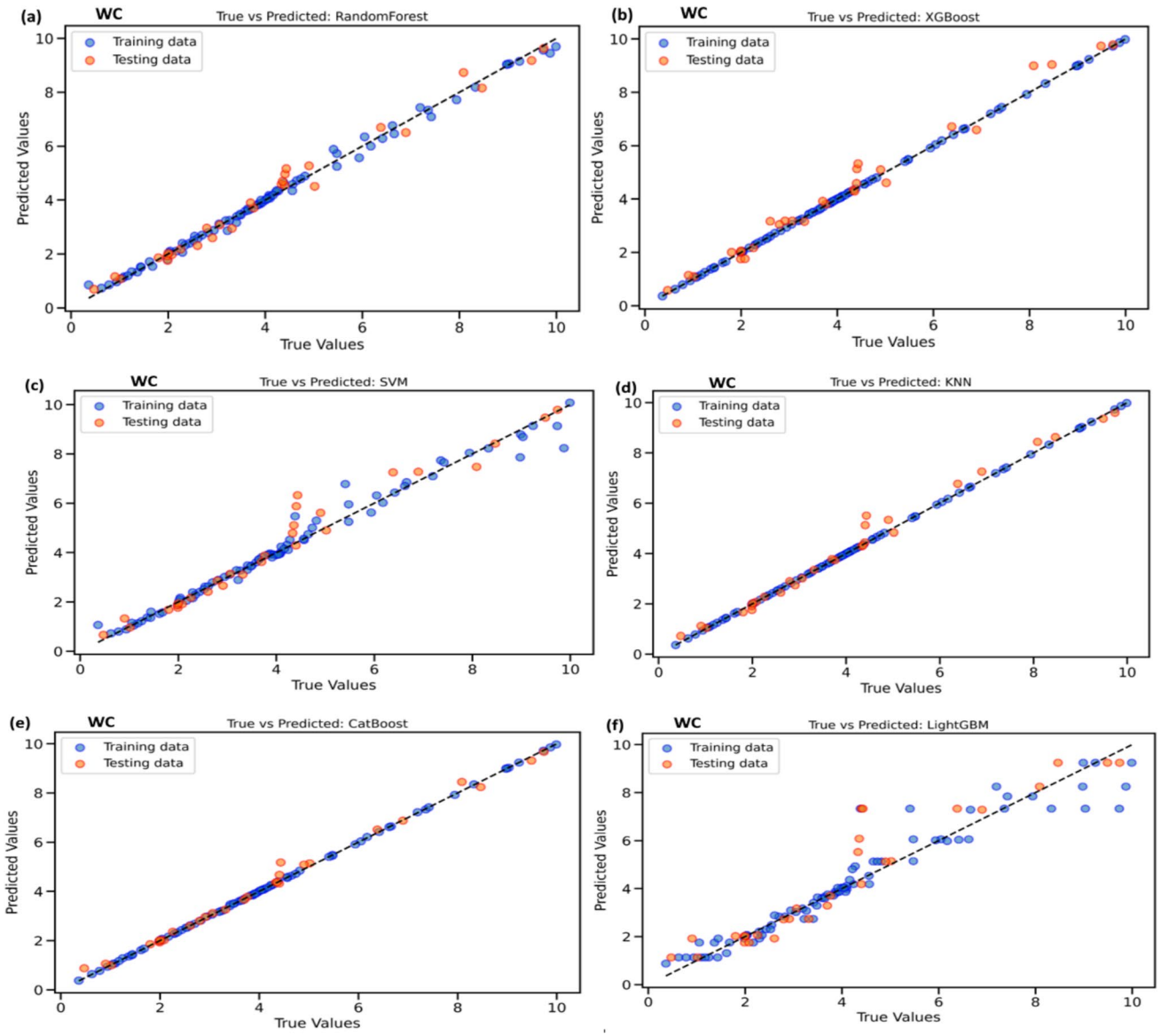

Fig. 13 True vs. Predicted scatter plots for WC across six ML models (**a**) RF, (**b**) XGBoost, (**c**) SVM, (**d**) KNN, (**e**) CatBoost, (**f**) LightGBM

also shows substantial variability and inconsistency, likely due to overfitting or sensitivity to outliers.

The residual distributions of six ML models - XGBoost, RF, SVM, KNN, CatBoost, and LightGBM - under WC conditions indicate significant differences in dispersion and symmetry, as illustrated in Fig. 14. CatBoost has a compact residual distribution with a mild positive skew and less variability, offering high accuracy for medium-grained but reduced accuracy for coarse-grained granite rock specimens. LightGBM shows the widest residual range and characterized by a significant negative skew, highlighting overprediction errors for coarse-grained granite. RF and XGBoost demonstrate a relatively symmetrical residual distribution centered around zero and with better prediction accuracy for fine grained rock specimens. However, XGBoost displays a slightly less variability than RF. In contrast, SVM and KNN exhibit skewed residual distributions, reflecting challenges in handling the heterogeneity of coarse-grained granite. The SVM residuals are positively skewed, characterized by a higher concentration of residuals near zero and an extended tail on the positive side, suggesting occasional underpredictions. The residuals of the KNN model tend to be skewed with predominantly clustering around zero and with a very limited variance. To sum it all up, all models are different in residual spread and skewness, with XGBoost and RF having more balanced distributions and the SVM, CatBoost and LightGBM having skewed distribution and varying error concentration.

The residual analysis across both FC and WC methods highlights varying degree of predictive accuracy of used models and most of these used models displayed heterogeneous model performance at extreme values. To further improve the understanding of the models' extensive predictive efficacy, we employed Taylor diagrams for both furnace cooling (FC) and water cooling (WC) conditions.

The Taylor diagram (Fig. 15) depict the correlation, variability, and discrepancies between observed and predicted porosity values. The models evaluated include RF, XGBoost, SVM, KNN, CatBoost, and LightGBM, with the observed data represented by the red point. For furnace cooling (FC), all models demonstrate high correlation coefficients (> 0.97) with the actual data, clustering tightly near the normalized standard deviation of 1.0. This indicates excellent prediction accuracy across all models, with minimal variance in their performance. The LightGBM model shows slightly higher standard deviation, suggesting minor overprediction tendencies.

Water cooling (WC) predictions displayed similar high correlation patterns, though with slightly more dispersed model performances. The correlation coefficients remain above 0.97, but the standard deviation spread is marginally wider compared to FC predictions. This increased spread likely reflects the more complex dynamics inherent in WC processes. This demonstrates the behavior of rocks under different cooling techniques: FC promotes the development of more uniform structures in medium and coarse grains via gradual cooling, while WC results in irregular porosity patterns and internal stresses, especially in fine grains, due to quenching effect. While the Taylor diagrams provided insights into the models' overall performance metrics, understanding the behavior of key variables driving these predictions is crucial. To elucidate this, we conducted SHAP (SHapley Additive exPlanations) analysis as shown

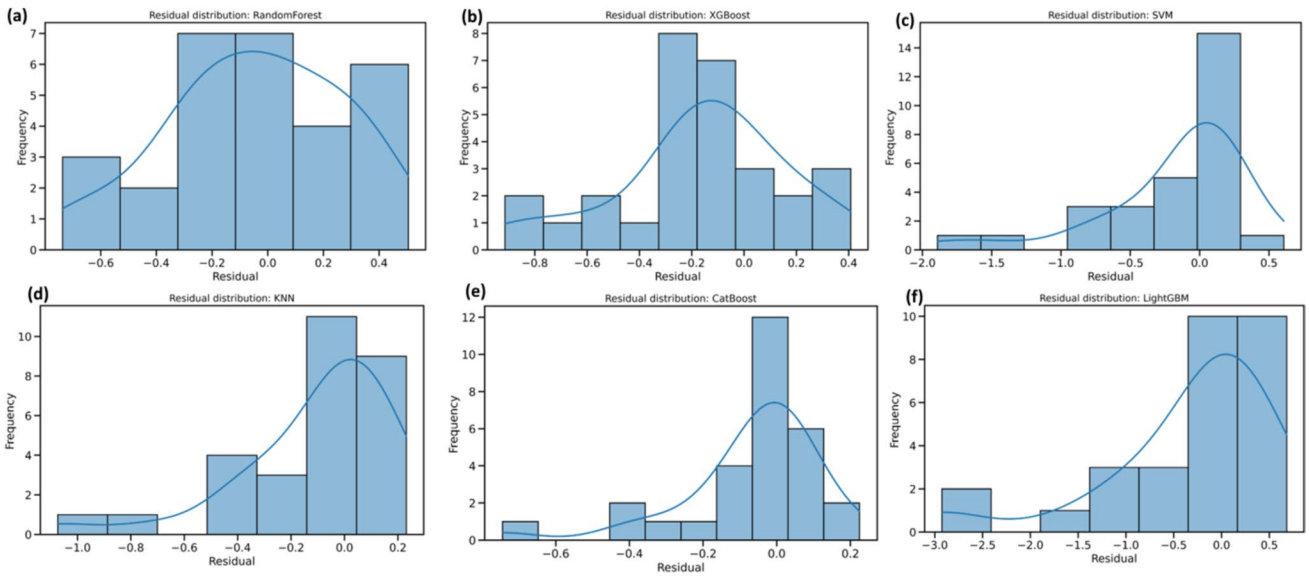

Fig. 14 Residual distribution for WC across six ML models (**a**) RF, (**b**) XGBoost, (**c**) SVM, (**d**) KNN, (**e**) CatBoost, (**f**) LightGBM

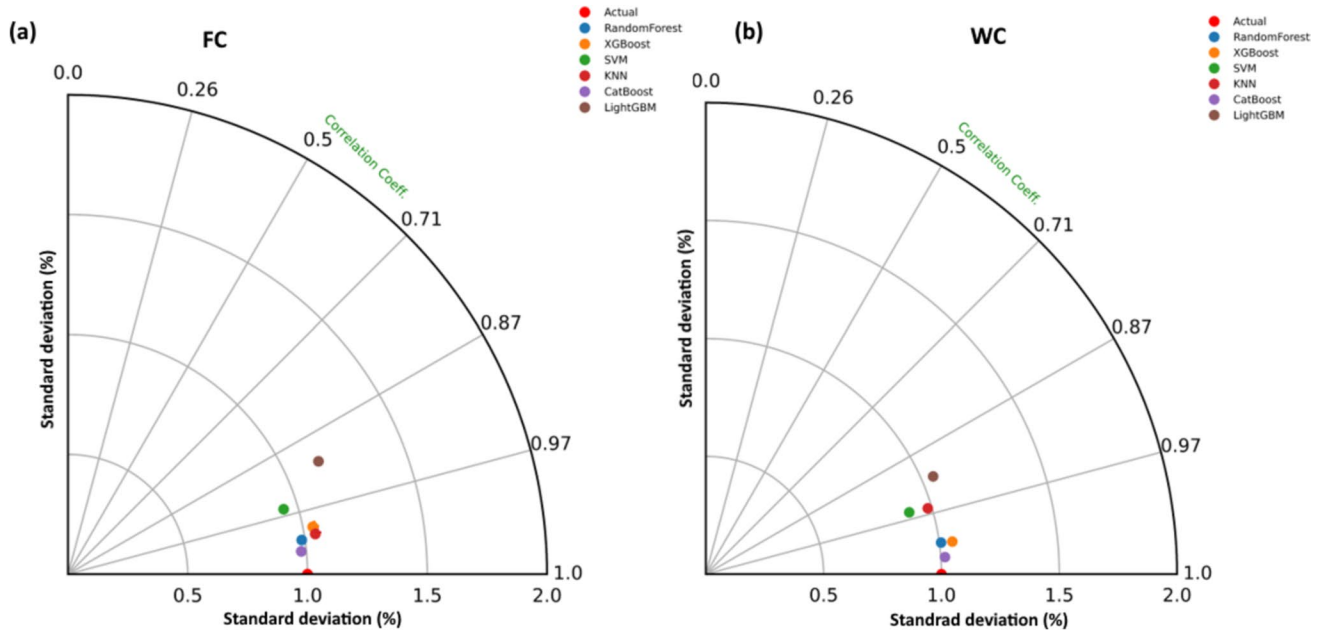

Fig. 15 Boxplots and Violin plots for FC and WC

in Fig. 16 to quantify and visualize the importance of factors affecting the porosity across both cooling conditions.

The analysis of the SHAP plot elucidate critical insights regarding the factors that influence the granite porosity under two separate cooling methods, FC and WC. In both methods, temperature (Feature 0) is found to be the most relevant variable, indicating that heating-cooling thermal effect has a significant impact on the porosity of granite. The induced thermal stress and microcrack formation is mainly governed by the temperature are directly related to porosity variation during heating-cooling processes.

Mass (Feature 1) is the second most important feature for both FC and WC, indicating that the physical dimensions or mass of the granite samples also affects the porosity of the granite rocks, mainly due to uneven temperature gradients and induced thermal stresses. P-wave velocity (Feature 2) that represents elasticity and micro-structural integrity is shown to have much higher SHAP impact under WC than in FC, indicating the impact of thermal shock in modifying the internal microstructure of the rock. This suggest that rapid quenching has a great impact on the internal microstructure of the granite, induces more abrupt thermal shock than gradual furnace cooling, and is therefore likely to facilitate more severe fracture formation and increased porosity. The residual features, comprising grain size coarse-grained (Feature 3), fine-grained (Feature 4), and medium-grained (Feature 5), exert a negligible influence on porosity prediction for both the cooling methods. This indicates that, although grain size affects rock characteristics, its impact on porosity is subordinate to temperature, mass, p-wave velocity, and structural changes induced by rapid or progressive cooling processes.

Overall, temperature, mass and p-wave velocity are the main determining factors of granite porosity, with temperature being the most influential across both cooling methods. These findings reveal the interaction of thermal, physical and elastic factors in controlling porosity progression under different cooling methods.

Sensitivity analysis

In rock mechanics it is important to understand the interactions and behavior of the various key variables, temperature, mass, and wave velocity. These factors significantly influence the physical and mechanical properties of the rocks. To analyze these complex relations, Partial Dependence Plots (PDPs or PD plot) and Individual Conditional Expectation (ICE) plots are valuable tools. PDPs reveal the marginal effect of one or two features on the ML model's prediction. These plots help to identify linear, monotonic, or non-linear patterns between input features and the target variables. ICE plots, on the other hand, depict detailed insights by capturing individual response at the data point level, revealing heterogeneity in the dataset. Therefore, this analysis demonstrate that these PDPs and ICE plots complement each other in understanding the impact of input features on the target variable, as illustrated in Fig. 17.

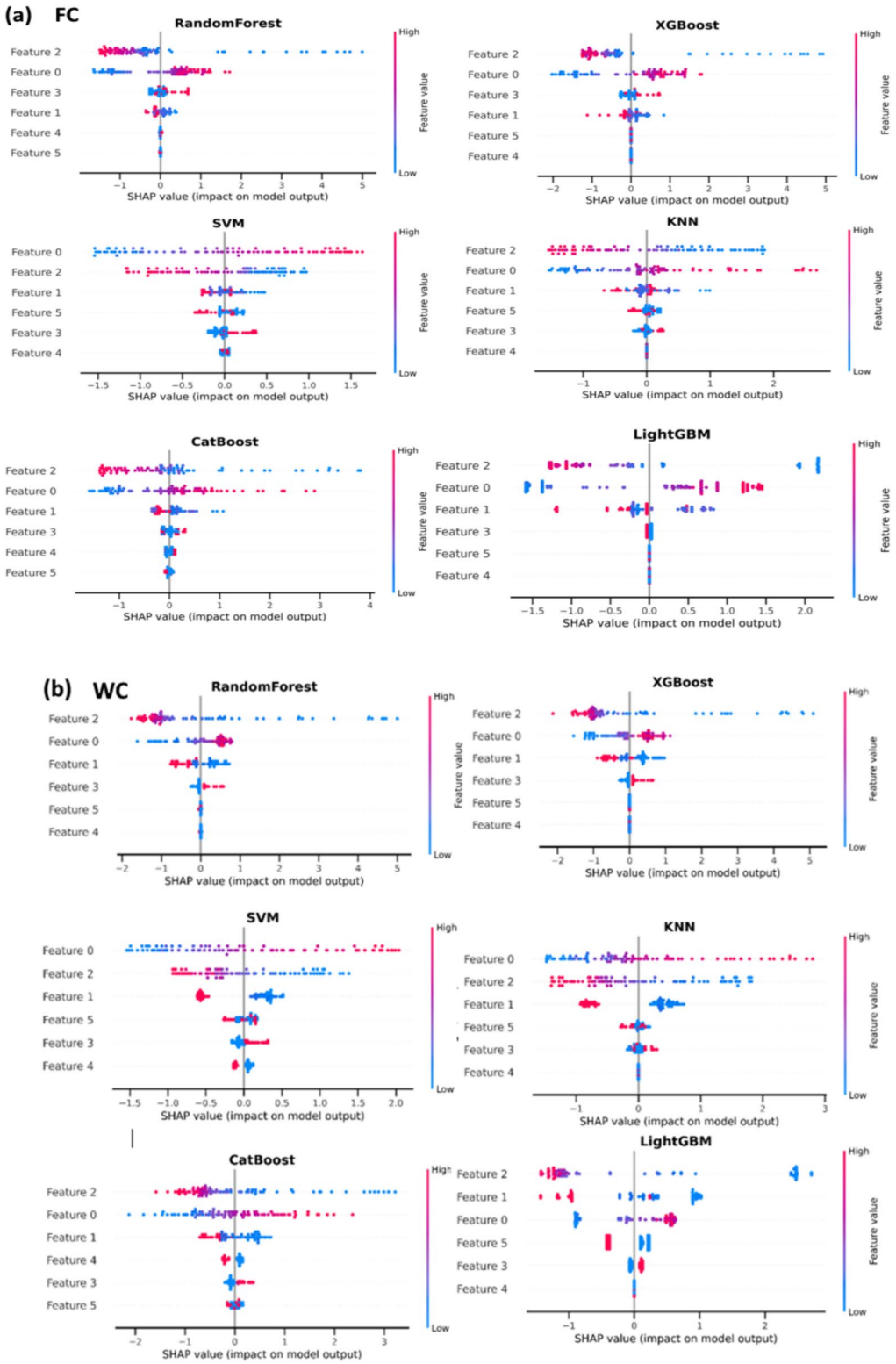

Fig. 16 SHAP analysis (**a**) FC (**b**) WC

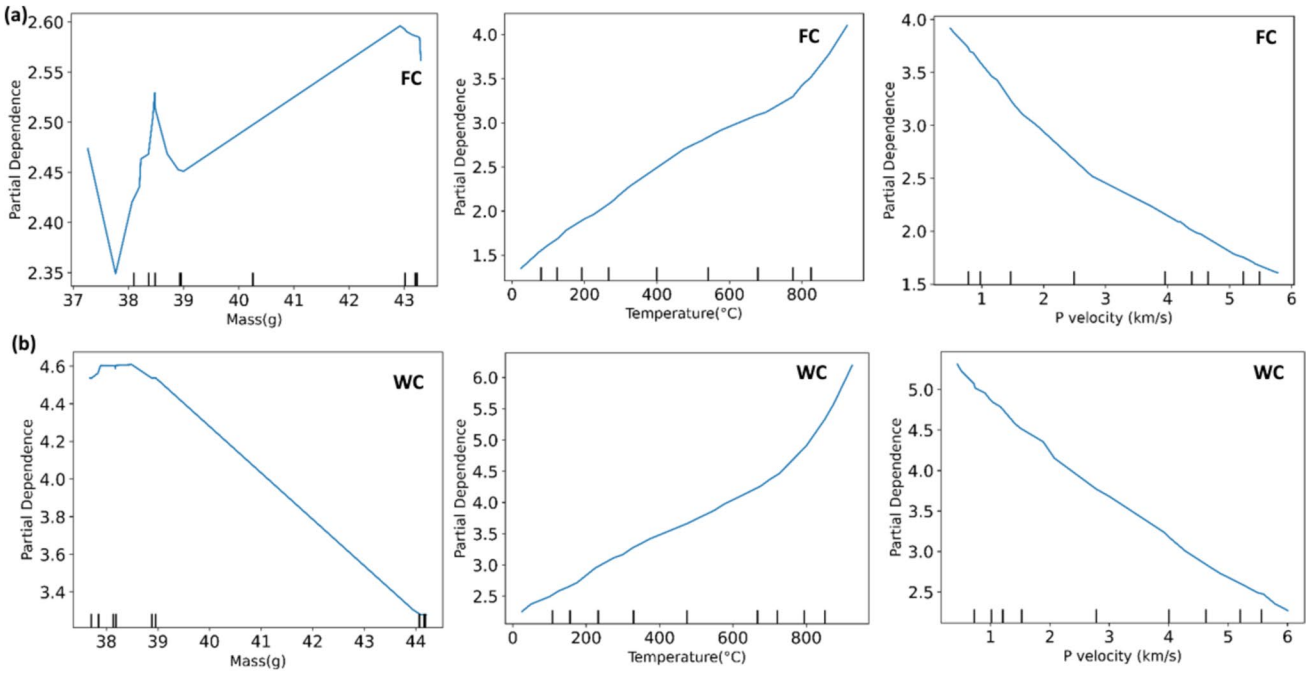

Fig. 17 1-Way PDP plot for (**a**) FC and (**b**) WC

The one-way PDP analysis

The one-way PDP were used to refer to how a single feature impacts the model prediction while holding the other features constant. Temperature plays a critical role in altering the physical and mechanical properties of rocks. Granite expands when heated and contracts during cooling. The gradual slow cooling, i.e., FC, shows slow uniform thermal contraction due to minimal changes in thermal expansion coefficient of constituting minerals, induces slight microcracking. However, in contrast, WC is characterized by rapid and significant induced thermal stress leads to increased effective thermal expansion, causes extensive microcracking.

Similarly, the mass of the rock specimens, reflecting its density and volume, affects its mechanical behavior. The one-way PDP for mass depicts a non-linear relationship with the porosity of rock, as shown in Fig. 17. Granite undergoes a minimal effect due to the gradual cooling process, primarily attributed to minor thermal expansion, which preserves the structural integrity of rock and caused slight reduction in density. Instead, rapid WC induces thermal shock, leading to extensive microcracks which caused significant increase in porosity and reduction in density. Fine-grained granite undergoes uniform expansion, causing a gradual decrease in density. In contrast, coarse-grained granite experiences more extensive microcracking and pore development, resulting in more prominent reduction in density.

The elastic properties and structural integrity of rock depend on p-wave velocity. It depicts a negative correlation with rock porosity. Due to increased porosity and microcracking, p-wave and s-wave velocity decrease with temperature. (Fig. 17). Fine-grained granite treated during thermal treatment retains its higher p-wave velocities due to its uniform microstructure, minimizing microcracking. Medium-grained granite shows a moderate decline in p-wave velocity. Instead, coarse-grained granite experiences the steepest decline in p-wave velocity due to induced extensive microcracking and increased porosity.

The two-way PDP analysis

The interaction between temperature and mass reveals a complex behavior under different cooling conditions (Fig. 18). For furnace-cooled rock specimens, increasing mass has a negligible effect on the porosity values. In contrast, water-cooled rock specimens exhibit a significant interaction between mass and temperature. At lowered temperatures, both reduced mass and temperature correspond to lower porosity. However, at elevated temperatures this effect diminishes due to the intensification of induced thermal cracking. This observation underscores the importance of considering the mass and temperature together, specially in thermally stressed system. The thermal expansion of granite is significantly dependent on the expansion coefficients of its constituent minerals and the grain size of the rock. Fine grained granite, with densely packed small grains, shows limited thermal expansion due to intergranular constraints. Medium grained granite has moderate thermal expansion for

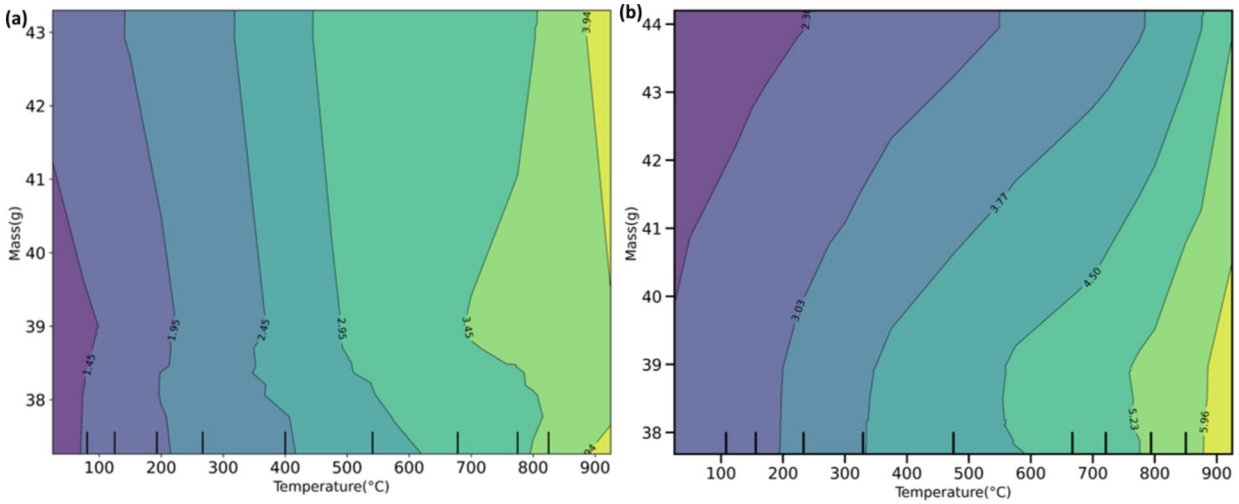

Fig. 18 2-way PDP between temperature and mass for (**a**) FC and (**b**) WC

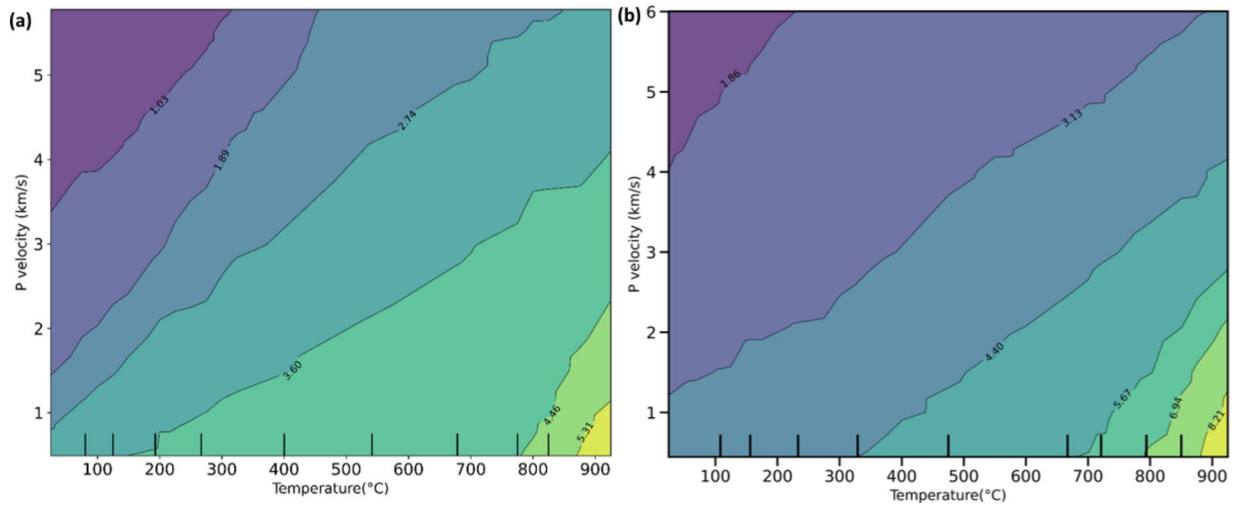

Fig. 19 2-way PDP between temperature and p-wave velocity for (**a**) FC and (**b**) WC

relatively larger grain boundaries. Instead, coarse-grained granite experiences the significant grain boundary displacement leads to greatest thermal expansion. Cooling methods further influences these effects; as FC encourages gradual and controlled contraction while WC causes thermal shock and uneven contraction, and extensive microcracking.

Temperature and p-wave velocity are interlinked, as higher p-wave velocities can partially limit the negative effect induced by the sudden rise and abrupt fall of the temperature, as illustrated in Fig. 19. The rocks with higher p-wave velocity provide better resistance against induced thermal stress. Nevertheless, beyond a certain temperature, extensive thermal cracking leads to significantly increase in porosity regardless of velocity. The interaction of mass and P wave velocity suggest that rocks with greater mass and p-wave velocity would have a lower porosity due to higher density and few internal flaws (Fig. 20). Although, these marginal benefits diminish at very high values, this suggests a saturation point where further increases in mass or p-wave velocity result in incremental improvements in porosity.

The mismatch in thermal expansion and contraction of constituting mineral grains causes an increase in porosity. During gradual FC, minor porosity change occurs due to limited induced thermal stress. In contrast, quenching induces high thermal stress during WC leads to extensive microcracking and significant increase in pore volume.

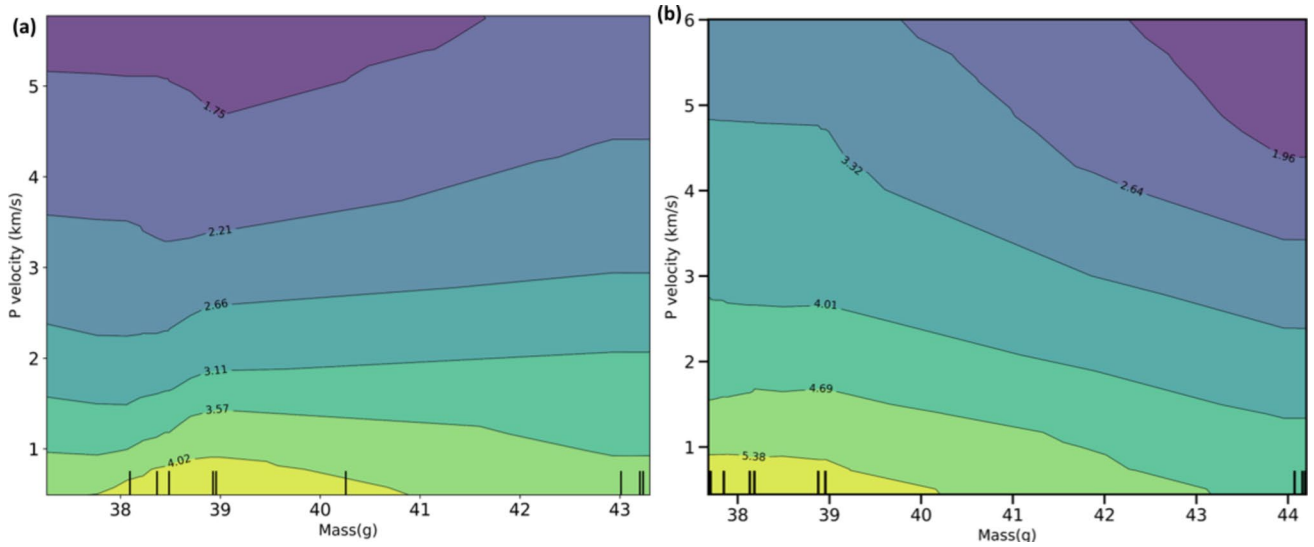

Fig. 20 2-way PDP between mass and p-wave velocity for (**a**) FC and (**b**) WC

Limitations of PDPs

PDPs for both furnace and water-cooling systems elucidate the average impacts of temperature, p-wave velocity, and mass on the target variable; still, they display significant limitations. PDPs assume independence of characteristics, which may not be valid in complex systems where interactions and correlations among variables occur. PDPs solely record the marginal impacts of characteristics, averaging the diversity and heterogeneity in individual predictions, hence concealing localized interactions and fluctuations within the dataset. This disadvantage is particularly apparent when contrasting FC and WC effects, as PDPs do not accurately represent the intricacies of thermal stress-induced alterations at the microstructural level, particularly in heterogeneous materials such as granite.

Thus, PDPs may reduce the complexity of the interactions among thermal, physical, and mechanical features, underscoring the necessity for supplementary tools like Individual Conditional Expectation (ICE) plots to elucidate feature impacts with greater specificity. ICE plots address the shortcomings of Partial Dependence Plots (PDPs) by illustrating the model's prediction for each individual data point as the feature of interest varies.

This method elucidates variability and heterogeneity in feature effects, offering a more comprehensive and nuanced view of their impact, as illustrated in Fig. 21. At an even granular level, temperature and p-wave velocity exhibit a consistent trend, indicating minimal interaction with other variables in the porosity prediction process. The divergence of the individual data point from the average values leads to an inconsistent mass, which in turn exhibits significant interaction with other features.

The comparison of ICE plots (blue lines) and PDPs (red dotted lines) for furnace and water cooling demonstrates significant disparities in feature effects and their variability among individual data points. The ICE plots for temperature during FC demonstrate a continuous upward trend that roughly corresponds with the PDP, signifying a relatively uniform effect of temperature on the objective variable. Likewise, the ICE plots for mass and p-wave velocity exhibit negligible deviations from the PDP, indicating restricted heterogeneity and interaction effects. Conversely, water cooling generates considerable variability and heterogeneity, especially regarding temperature and mass, as demonstrated by the increased divergence of the ICE trajectories from the average PDP. In terms of temperature, the PDP exhibits a steady rise, whereas the ICE plots reveal sudden fluctuations and erratic patterns, signifying localized non-linear effects during rapid cooling circumstances.

The ICE plots for mass further highlight this variability, with significant differences among individual data points. Regarding p-wave velocity, both cooling methods provide a continuous negative trend; however, the ICE plots for water cooling indicate steeper gradients and greater variability, highlighting the intensified thermal stresses and varied reactions caused by rapid cooling. Water cooling results in increased unpredictability and non-linear interactions in feature effects, in contrast to the consistent and predictable behavior seen with furnace cooling. This underscores the importance of ICE plots for obtaining detailed, instance-level insights that may be overlooked by PDPs alone.

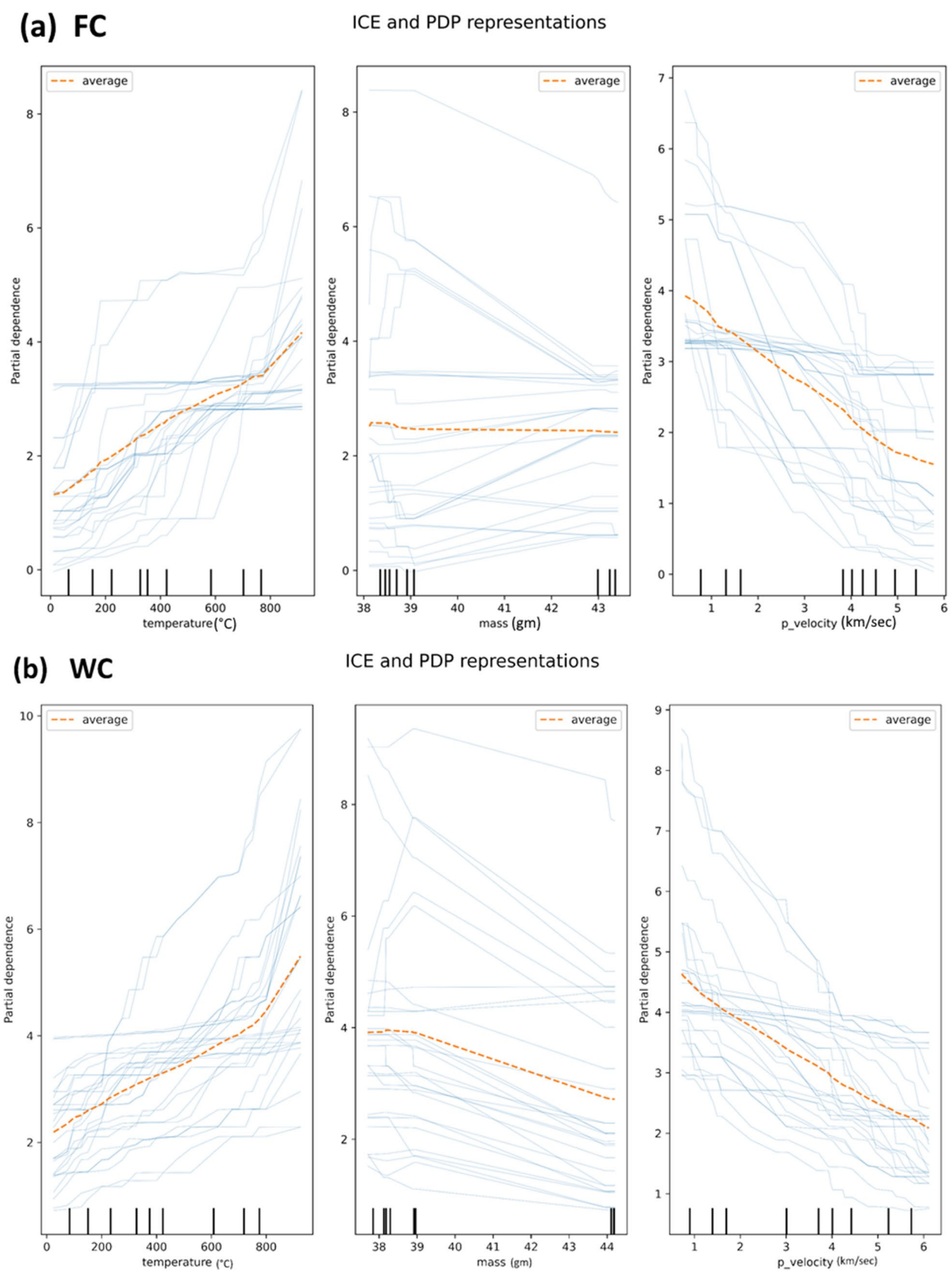

Fig. 21 PDP (dashed line) and ICE plots for (**a**) furnace cooling and (**b**) water cooling

Conclusion

This study has analyzed the application of six different machine learning methods to estimate the granite porosity at elevated temperature and various cooling rate. The comprehensive outcomes of the present study are discussed below:

1) FC leads to gradual thermal contraction, resulting in fewer microcracks and higher wave velocities. In contrast, WC induces thermal shock, generating steep thermal gradient. This cause extensive microcracking, increasing porosity and reducing wave velocities.
2) Grain size of constituting minerals of the granite certainly affects the induced thermal stress response. Fine-grained granite resists induced thermal stress cracking due to the smaller grain boundaries, maintaining comparatively lower porosity. Medium-grained granite displays moderate changes, with some microcracking. Coarse-grained granite, with larger grain boundaries, experiences severe induced thermal stress causing extensive microcracking which results as increased porosity.
3) The comparative study of the six different ML models used for the porosity prediction of granite treated at various heating-cooling conditions classifies CatBoost as the most precise and reliable model. RF and KNN which effectively capture the complex non-linear relationships, exhibit strong predictive performance. XGBoost also demonstrate reasonably good performance but with small overestimation. On the other hand, SVM and LightGBM struggle in dealing with data heterogeneity.
4) The combination of PDPs and ICE plots reveals the critical roles of temperature, mass, and p-wave velocity on granite porosity. These plots elucidates both average effects and localized variability, providing important information on nonlinear interaction of these variables in thermally stressed systems. Temperature induces thermal expansion and microcracking, mass reflects density-related microstructural changes, and p-wave velocity indicates elastic integrity.
5) It was observed that ML methods, when properly tuned and validated, can effectively predict the porosity of granite under varying heating-cooling conditions, providing valuable insights for enhanced geothermal systems.

Author contributions RD: Research Conceptualization, Experimental investigation, Data Collection, Methodology Development, Data Analysis, Manuscript Writing, Editing and ReviewBP: Data Collection, Methodology Development, Data Analysis, reviewPKG: Research Conceptualization, Experimental investigation, Data Collection, Methodology Development, Data Analysis, Manuscript Writing, Editing and ReviewPG: Data Collection, Methodology Development, Review, Data AnalysisSD: Editing and Review, SupervisionKHS: Editing and Review, SupervisionTNS: Editing and Review, Supervision.

Funding statement This study was financial supported by a fellowship from the Council of Scientific and Industrial Research (CSIR). The fellowship was awarded to the first author.

Data availability No datasets were generated or analysed during the current study.

Declarations

Competing interests The authors declare no competing interests.

Conflict of interest The authors have declared that there is no conflict of interest in this submitted manuscript.

References

Bonazza A, Sabbioni C, Messina P et al (2009) Climate change impact: mapping thermal stress on Carrara marble in Europe. Sci Total Environ 407:4506–4512

Breede K, Dzebisashvili K, Liu X, Falcone G (2013) A systematic review of enhanced (or engineered) geothermal systems: past, present and future. Geotherm Energy 1:1–27. https://doi.org/10.1186/2195-9706-1-4

Brotóns V, Tomás R, Ivorra S, Alarcón JC (2013) Temperature influence on the physical and mechanical properties of a porous rock: San Julian's calcarenite. Eng Geol 167:117–127. https://doi.org/10.1016/j.enggeo.2013.10.012

Browning J, Meredith P, Gudmundsson A (2016) Cooling-dominated cracking in thermally stressed volcanic rocks. Geophys Res Lett 43:8417–8425. https://doi.org/10.1002/2016GL070532

Chauhan S, Rühaak W, Khan F et al (2016) Processing of rock core microtomography images: using seven different machine learning algorithms. Comput Geosci 86:120–128. https://doi.org/10.1016/j.cageo.2015.10.013

Chen Y, Watanabe K, Kusuda H et al (2011) Crack growth in Westerly granite during a cyclic loading test. Eng Geol 117:189–197. https://doi.org/10.1016/j.enggeo.2010.10.017

Chen YL, Ni J, Shao W, Azzam R (2012) Experimental study on the influence of temperature on the mechanical properties of granite under uni-axial compression and fatigue loading. Int J Rock Mech Min Sci 56:62–66. https://doi.org/10.1016/j.ijrmms.2012.07.026

Chen YL, Wang SR, Ni J et al (2017) An experimental study of the mechanical properties of granite after high temperature exposure based on mineral characteristics. Eng Geol 220:234–242. https://doi.org/10.1016/j.enggeo.2017.02.010

Chen G, Wang J, Li J et al (2018) Influence of temperature on crack initiation and propagation in granite. Int J Geomech 18:4018094. https://doi.org/10.1061/(asce)gm.1943-5622.0001182

Eltarabily MG, Elshaarawy MK (2023) Risk assessment of potential groundwater contamination by agricultural drainage water in the Central Valley Watershed, California, USA. In Groundwater Quality and Geochemistry in Arid and Semi-Arid Regions. Springer Nature Singapore, Cham, pp 37–76. https://link.springer.com/chapter/10.1007/698_2023_1051

Elshaarawy M, Eltarabily MG (2024) Machine learning models for predicting water quality index: optimization and performance analysis for El Moghra, Egypt. Water Supply 24:3269–3294. https://doi.org/10.2166/ws.2024.189

Elshaarawy MK, Hamed AK (2024) Stacked ensemble model for optimized prediction of triangular side orifice discharge coefficient. Eng Optim. https://doi.org/10.1080/0305215X.2024.2397431

Eltarabily MG, Abd-Elhamid HF, Zeleňáková M et al (2023) Predicting seepage losses from lined irrigation canals using machine learning models. Front Water 5:1287357. https://doi.org/10.3389/frwa.2023.1287357

Elshaarawy MK, Alsaadawi MM, Hamed AK (2024) Machine learning and interactive GUI for concrete compressive strength prediction. Sci Rep 14:1–26. https://doi.org/10.1038/s41598-024-66957-3

Eltarabily MG, Elshaarawy MK, Elkiki M, Selim T (2024a) Computational fluid dynamics and artificial neural networks for modelling lined irrigation canals with low-density polyethylene and cement concrete liners. Irrig Sci 73:910–927. https://doi.org/10.1002/ird.2911

Eltarabily MG, Selim T, Elshaarawy MK, Mourad MH (2024b) Numerical and experimental modeling of geotextile soil reinforcement for optimizing settlement and stability of loaded slopes of irrigation canals. Environ Earth Sci 83:1–15. https://doi.org/10.1007/s12665-024-11560-y

Fellner M, Supancic P (2002) Thermal shock failure of brittle materials. Key Eng Mater 223:97–106

Freire-Lista DM, Fort R, Varas-Muriel MJ (2016) Thermal stress-induced microcracking in building granite. Eng Geol 206:83–93. https://doi.org/10.1016/j.enggeo.2016.03.005

Gallup DL (2009) Production engineering in geothermal technology: a review. Geothermics 38:326–334. https://doi.org/10.1016/j.geothermics.2009.03.001

Gautam PK, Verma AK, Jha MK et al (2016a) Study of strain rate and thermal damage of Dholpur Sandstone at elevated temperature. Rock Mech Rock Eng 49:3805–3815. https://doi.org/10.1007/s00603-016-0965-5

Gautam PK, Verma AK, Maheshwar S, Singh TN (2016b) Thermo-mechanical analysis of different types of sandstone at elevated temperature. Rock Mech Rock Eng 49:1985–1993. https://doi.org/10.1007/s00603-015-0797-8

Gautam PK, Verma AK, Jha MK et al (2018a) Effect of high temperature on physical and mechanical properties of Jalore granite. J Appl Geophy 159:460–474

Gautam PK, Verma AK, Sharma P, Singh TN (2018b) Evolution of thermal damage threshold of Jalore granite. Rock Mech Rock Eng 51:2949–2956

Gautam PK, Jha MK, Verma AK, Singh TN (2019a) Evolution of absorption energy per unit thickness of damaged sandstone. J Therm Anal Calorim 136:2305–2318

Gautam PK, Verma AK, Singh TN et al (2019b) Experimental investigations on the thermal properties of Jalore granitic rocks for nuclear waste repository. Thermochim Acta 681:178381

Gautam PK, Dwivedi R, Kumar A et al (2021) Damage characteristics of jalore granitic rocks after thermal cycling effect for nuclear waste repository. Rock Mech Rock Eng 54:235–254

Heuze FE (1983) High-temperature mechanical, physical and thermal properties of granitic rocks- A review. Int J Rock Mech Min Sci 20:3–10. https://doi.org/10.1016/0148-9062(83)91609-1

Hu X, Shentu J, Xie N, Huang Y, Lei G, Hu H, Gong X (2023) Predicting triaxial compressive strength of high-temperature treated rock using machine learning techniques. J Rock Mech Geotech Eng 15(8):2072–2082

Isaka BLA, Gamage RP, Rathnaweera TD et al (2018) An influence of thermally-induced micro-cracking under cooling treatments: mechanical characteristics of Australian granite. Energies (Basel) 11:1338

Isleem HF, Tang Q, Alsaadawi MM (2024) Numerical and machine learning modeling of GFRP confined concrete-steel hollow elliptical columns. Sci Rep. https://www.nature.com/articles/s41598-024-68360-4

Jha MK, Verma AK, Gautam PK, Negi A (2017) Study of mechanical properties of Vindhayan shaly rocks at elevated temperature. J Geol Soc India 90:267–272. https://doi.org/10.1007/s12594-017-0714-8

Kang F, Li Y, Tang C (2021) Grain size heterogeneity controls strengthening to weakening of granite over high-temperature treatment. Int J Rock Mech Min Sci 145:10484. https://doi.org/10.1016/j.ijrmms.2021.104848

Kim K, Kemeny J, Nickerson M (2014) Effect of rapid thermal cooling on mechanical rock properties. Rock Mech Rock Eng 47:2005–2019. https://doi.org/10.1007/s00603-013-0523-3

Kumari WGP, Ranjith PG, Mba P et al (2017) Temperature-dependent mechanical behaviour of Australian strathbogie granite with different cooling treatments. Eng Geol 229:31

Kumari WGP, Ranjith PG, Perera MSA, Chen BK (2018) Experimental investigation of quenching effect on mechanical, microstructural and flow characteristics of reservoir rocks: thermal stimulation method for geothermal energy extraction. J Pet Sci Eng 162:419–433. https://doi.org/10.1016/j.petrol.2017.12.033

Liu S, Xu J (2015) An experimental study on the physico-mechanical properties of two post-high-temperature rocks. Eng Geol 185:63–70. https://doi.org/10.1016/j.enggeo.2014.11.013

Liu H, Zhang K, Shao S, Ranjith PG (2019) Numerical investigation on the mechanical properties of Australian strathbogie granite under different temperatures using discrete element method. Rock Mech Rock Eng 52:3719–3735

Mahmoodzadeh A, Nejati HR, Mohammadi M et al (2022) Prediction of Mode-I rock fracture toughness using support vector regression with metaheuristic optimization algorithms. Eng Fract Mech 264:4. https://doi.org/10.1016/j.engfracmech.2022.108334

Miah MI, Ahmed S, Zendehboudi S, Butt S (2020) Machine learning approach to model rock strength: prediction and variable selection with aid of log data. Rock Mech Rock Eng 53:4691–4715. https://doi.org/10.1007/s00603-020-02184-2

Shao S, Wasantha PLP, Ranjith PG, Chen BK (2014) Effect of cooling rate on the mechanical behavior of heated strathbogie granite with different grain sizes. Int J Rock Mech Min Sci 70:381–387. https://doi.org/10.1016/j.ijrmms.2014.04.003

Shi X, Gao L, Wu J et al (2020) Effects of cyclic heating and water cooling on the physical characteristics of granite. Energies (Basel) 13:99–110. https://doi.org/10.3390/en13092136

Siratovich PA, Villeneuve MC, Cole JW et al (2015) Saturated heating and quenching of three crustal rocks and implications for thermal stimulation of permeability in geothermal reservoirs. Int J Rock Mech Min Sci 80:265–280. https://doi.org/10.1016/j.ijrmms.2015.09.023

Song Z, Zhang Z, Zhang G et al (2022) Identifying the types of loading mode for rock fracture via convolutional neural networks. J Geophys Res Solid Earth 127:2. https://doi.org/10.1029/2021JB022532

Su G, Chen Z, Ju JW, Jiang J (2017) Influence of temperature on the strainburst characteristics of granite under true triaxial loading conditions. Eng Geol 222:38–52. https://doi.org/10.1016/j.enggeo.2017.03.021

Tian W, Isleem HF, Hamed AK, Elshaarawy MK (2024) Enhancing discharge prediction over Type-A piano key weirs: an innovative machine learning approach. Flow Meas Instrum 100:102732. https://doi.org/10.1016/j.flowmeasinst.2024.102732

Wang L, Wu C, Tang L et al (2020) Efficient reliability analysis of earth dam slope stability using extreme gradient boosting method. Acta Geotech 15:3135–3150. https://doi.org/10.1007/s11440-020-00962-4

Wang YT, Zhang X, Liu XS (2021) Machine learning approaches to rock fracture mechanics problems: Mode-I fracture toughness determination. Eng Fract Mech 253:10789. https://doi.org/10.1016/j.engfracmech.2021.107890

Wei M, Meng W, Dai F, Wu W (2022) Application of machine learning in predicting the rate-dependent compressive strength of rocks. J Rock Mech Geotech Eng 14:1356–1365. https://doi.org/10.1016/j.jrmge.2022.01.008

Weidner L, Walton G, Kromer R (2019) Classification methods for point clouds in rock slope monitoring: a novel machine learning approach and comparative analysis. Eng Geol 263:6. https://doi.org/10.1016/j.enggeo.2019.105326

Weng L, Wu Z, Liu Q (2020) Influence of heating/cooling cycles on the micro/macrocracking characteristics of Rucheng granite under unconfined compression. Bull Eng Geol Environ 79:1289–1309. https://doi.org/10.1007/s10064-019-01638-4

Wu X, Huang Z, Cheng Z et al (2019a) Effects of cyclic heating and LN2-cooling on the physical and mechanical properties of granite. Appl Therm Eng 156:99–110

Wu X, Huang Z, Song H et al (2019b) Variations of physical and mechanical properties of heated granite after rapid cooling with liquid nitrogen. Rock Mech Rock Eng 52:2123–2139. https://doi.org/10.1007/s00603-018-1727-3

Xie C, Nguyen H, Bui XN et al (2021) Predicting rock size distribution in mine blasting using various novel soft computing models based on meta-heuristics and machine learning algorithms. Geosci Front 12:101108. https://doi.org/10.1016/j.gsf.2020.11.005

Yan H, Zhang J, Zhou N et al (2021) Crack initiation pressure prediction for SC-CO2 fracturing by integrated meta-heuristics and machine learning algorithms. Eng Fract Mech 249:107750

Zhao Z (2016) Thermal influence on mechanical properties of granite: a microcracking perspective. Rock Mech Rock Eng 49:747–762. https://doi.org/10.1007/s00603-015-0767-1

Zhao Z, Liu Z, Pu H, Li X (2018) Effect of thermal treatment on Brazilian tensile strength of granites with different grain size distributions. Rock Mech Rock Eng 51:1293–1303. https://doi.org/10.1007/s00603-018-1404-6

Zhou C, Wan Z, Zhang Y, Gu B (2018) Experimental study on hydraulic fracturing of granite under thermal shock. Geothermics 71:146–155